Improving Bioanalytical Methods of miRNA Analysis and its Applications to Breast Cancer

By
Victoria Tran

A PROJECT

submitted to

Oregon State University

University Honors College

in partial fulfillment of
the requirements for the
degree of

Honors Baccalaureate of Science in Biology
(Honors Associate)

Presented May 28th, 2015
Commencement June 2015

AN ABSTRACT OF THE THESIS OF

Victoria Tran for the degree of Honors Baccalaureate of Science in Biology presented on May 28th, 2015. Title: Improving Bioanalytical Methods of miRNA Analysis and its Applications in Breast Cancer.

Abstract approved:

_____

Sean M. Burrows

Micro-ribonucleic acids (miRNA) are becoming an increasingly popular topic of research in hopes of discovering newfound biomarkers and/or therapies for numerous types of cancers and diseases. MiRNA are a type of biomolecule contributing to the progression of multiple cancers and diseases, and such biomolecules are called biomarkers. Current RNA-based biosensors suffer from various flaws such as slow analysis, false signals, sensitivity or the lack of fine-tuned selectivity. The reporter-probe biosensor presented here demonstrates great potential in resolving some of these issues. The biosensor consists of a fluorescent reporter molecule bound to a probe that is more selective for a miRNA than the reporter. The sensor works by simultaneously forming a probe-miRNA target complex and displacing the reporter. The freed reporter is then able to bind to itself using intramolecular forces, forming a hairpin structure inducing a fluorescent signal change. This change in analytical signal can then be measured and related to presence or absence determination and quantification of the miRNA. This innovative miRNA reporter-probe biosensor design is not only capable of reducing false positives, demonstrating selectivity towards three miRNA, but is highly sensitive, a key component to a good biosensor due to the natural low levels (Femtomolar and nanomolar) of miRNA expression in the body. The results of my work have contributed to ongoing studies in the Burrows Lab to one day design an optimal biosensor demonstrating all these feats.

Key Words: Biosensor, reporter-probe complex, probe-target complex, hairpin conformation, fluorescence resonance energy transfer (FRET), quenching, false signals, sensitivity, selectivity, and micro-ribonucleic acid (miRNA)

Corresponding email address: tranvic@onid.oregonstate.edu

Improving Bioanalytical Methods of miRNA Analysis and its Applications to Breast Cancer

By
Victoria Tran

A PROJECT

submitted to

Oregon State University

University Honors College

in partial fulfillment of
the requirements for the
degree of

Honors Baccalaureate of Science in Biology
(Honors Associate)

Presented May 28th, 2015
Commencement June 2015

Honors Baccalaureate of Science project of Victoria Tran presented on May 28th, 2015.

APPROVED:

Sean M. Burrows, Mentor, representing Department of Chemistry

Siva K. Kolluri, Committee Member, representing Department of Environmental & Molecular Toxicology

Nicholas Larkey, Committee Member, representing Department of Chemistry

Toni Doolen, Dean, University Honors College

I understand that my project will become part of the permanent collection of Oregon State University, University Honors College. My signature below authorizes release of my project to any reader upon request.

Victoria Tran, Author

Acknowledgments

Thank you to the DeLoach Work Scholarship for funding a part of my thesis research. I would like to convey my deepest appreciation and thanks to all family, friends, and members of the Burrows research group for their continuing support. Their positive and friendly attitudes made the whole lab experience so much brighter. I want to specifically thank Dr. Siva K. Kolluri for taking the time and being a part of my thesis committee, and I would also like to thank Nicholas Larkey for being such a remarkable and awesome graduate mentor to work with. Lastly, I want to specifically express my gratitude towards my mentor, Dr. Sean M. Burrows for all his patience, guidance, and kindness while working diligently to accomplish our goals together. It has been an honor to receive such a wonderful opportunity working the Burrows Lab. Thank you very much for all your cooperation in order to make this possible.

TABLE OF CONTENTS

Page

Introduction 1-7

Chapter 1: Validation of Reporter + Probe Biosensor to Detect Low Levels of miRNA and Mitigate False Signals. 8-23

Chapter 1 Introduction 9-15

Methods 8

Results & Discussion 16-22

Chapter 1 Conclusion 23

Chapter 2: Investigation of Two-Photon FRET Pairs and use of Carbon-Oxygen Spacers for Signal Enhancement using Linear Strands of DNA 24-46

Section 2.1: FRET pair studies on Linear DNA Strands 24-33

Methods 24-27

Results & Discussion 27-33

Section 2.2: FAM/Atto633 FRET Reporter-Probe Biosensor 34-39

Results & Discussion 34-37

Section 2.1 & Section 2.2 Conclusion 38-39

Section 3.0: Spacer Studies to Optimize Cy3/Cy5 FRET Efficiency 39-51

Methods 39-42

Results & Discussion 43-50

Section 3.0 Conclusion 50-51

Summary 51-53

References 54

LIST OF FIGURES

Figure Page

1.0 Visual of Experimental Set Up 5

1.1 Schematic of Designed Biosensor Recognition Mechanism 10

1.2 Fluorescence Emission of Reporter-Probe with Cy5 and Cy3 Fluorophores 12

1.3 Percent Change in Signal due to Nuclease Degradation.....15

1.4 Evaluation of Selectivity, Stability, and Biological Potential of Biosensor 17

1.5 Bar Graph of Average Background Corrected Summed Intensity of miR-26a or miR-27a with Analyte or Off-Analyte 18

2.1 Hybridization Reaction for FRET Studies 25

2.2 Percent Change in Signal for 5′Alex488, 5′Alex532, and 5′Cy5 Paired with Various FRET dyes 28

2.3 Average Background Corrected Summed Intensity of R25 Excitation Spectra with and without Spacers 35

2.4 Percent Change from R25 + P to R25 Using FAM and Atto633 37

3.1 Generic Hybridization Reaction for Spacer Study.....40

3.2 Dilution Scheme of Sample Preparation for Spacer Studies 41

3.3 Percent Enhancement in Relation to Spacer Length for 3′Cy3 and 5′Cy5 Pair.....43

3.4 Percent Enhancement Evaluation with Respect to Spacer Lengths of “0, 0”, “18, 9” and “18, 18” 45

3.5 Emission Spectra at 960 nm Excitation of 3′Cy3 and 5′Cy5 Pair with “0, 0”, “18, 9” and “18, 18” Spacers.....46

3.6 Emission Spectra at 740 nm excitation of 3′Cy3 and 5′Cy5 pair with “0, 0”, “18, 9” and “18, 18” spacers. 49

LIST OF TABLES

Figure Page

1.1 Table of Reporter, Probe1, Let-7a Target, Let-7a Variant, miR9 Sequences.....16

1.2 Analytical Figures of Merit for 100 nM Reporter-′probe Biosensors.....21

1.3 Reporter-probe Complex Calibration Curve Slopes of miR-26a, and miR-27 with 100 nM Analyte and without 100 nM Off-Analytes 22

2.1 Dyes, Oligonucleotide Sequence, and Dye Placement on Oligonucleotide 24

2.2 Dye-pair Combinations Investigated 26

2.3 Strongest and Weakest Quenching at Associated Excitation Wavelength for each Dye-pair Studied 30

3.1 Combinations of Paired 3′Cy3 and 5′Cy5 Heterodimers 40

Introduction

According to statistics provided by the American Cancer society, there will be an estimated 1.6 million new cases of cancer in 2015, and approximately half will be women and the other half men. Of the new cases estimated for women, at least 29% of them will be diagnosed as breast cancer. And of the number of cancer deaths, 15% are attributed to breast cancer. Approximately one in eight women will be at risk for developing breast cancer in their lifetime. Breast cancer has been trending as the number one leader in cancer incidence rates for women in the U.S. since 1975.[1]

Clinically many breast cancers are primarily detected by three protein biomarkers: estrogen receptor (ER), progesterone receptor (PR), and human epidermal growth factor receptor 2 (HER2). Unfortunately these biomarkers fail to detect aggressive breast cancers like triple negative breast cancers (TNBC). In fact TNBC means ER, PR, and HER are not detected. Mammograms fail to spot these cancers until it is too late. Many studies are showing miRNAs hold great potential as a biomarker of aggressive cancers. Thus, miRNA detection contains potential for early detection, therapeutic decision making, and targets for miRNA-based therapies. This type of cancer can be prevented if detected early on; a goal in which I strive to do by improving miRNA biosensor technology.

A biosensor is, "A self-contained analytical device that incorporates a biologically active material in intimate contact with an appropriate signaling mechanism for the purpose of detecting (reversibly and selectively) the concentration or activity of chemical species in any type of sample.[2]" There are various kinds of biosensors such as the molecular beacon technology or the double-strand technology.

Micro-ribonucleic acid (miRNA) is a family of small non-coding RNA, approximately ranging from 21 to 24 nucleotide bases. They carry a significant role in post-transcriptional regulation of gene expression[3], often by interacting with messenger-ribonucleic acid (mRNA). On the miRNA itself, contains a sequence called a "seed". This sequence has a complementary sequence named the "seed-match" on the target mRNA. The role of miRNA is to bind the mRNA and cause either degradation of the mRNA or inhibition of protein synthesis. The expression of miRNAs plays an important role in protein expression of biological processes like cellular proliferation, differentiation, and apoptosis (Programmed cell death).[4] Alterations in the normal expression of miRNA has been identified to be associated with the progression and regulation of multiple cancers such as thyroid, colorectal, prostate, ovarian, lung, and breast cancer. They are also prominent biomarkers in numerous diseases, for example, neurological or even immunological diseases.[5]

The main types of genes associated with miRNA regulation are tumor suppressor (TS) genes, as well as oncogenes. TS genes are those that signal the cell to stop growing and initiate programed cell death. It is problematic when miRNA is overexpressed because TS genes are downregulated—loss of expression. Without TS-based signals, the cell would continuously grow with no indication of ever dying. Underexpression of miRNAs is also problematic because the lack of miRNA to regulate oncogenes causes an overexpression of oncogenes, leading to uncontrollable cell growth. [6]

Highly conserved sequences, when compared in multiple animal species, demonstrate relatively minimal differences within the sequences. Such similarities spanning across numerous species indicates the necessity of the particular sequence

towards the preservation of life. Therefore, selecting a model miRNA that is active as well as conserved in many species is ideal when attempting to evaluate the efficacy of miRNA-based biosensors. Lethal-7 (Let-7a) is a cancer-regulating miRNA and was chosen for our initial studies due to its highly conserved nature. In addition, it has been connected to cell-based diseases.[5] There have been studies that have shown the Let-7a family miRNA were downregulated in multiple cancers.

There are over 20 miRNAs working behind the scenes of breast cancer. For instance, miR-20a is involved in cell invasion and proliferation; miR-21 is anti-apoptotic; miR-155 is involved in the transforming growth factor-β (TGF-β) induced epithelial mesenchymal transformation (EMT). Combination of miRNAs can also work cooperatively to produce larger effects: the miR-200 family along with miR-205, work in conjunction to downregulate E-cadherin transcriptional repressors, plus proteins involved in tumor metastasis and EMT.[4] EMT is a process some epithelial cells undergo allowing them to become migratory and possibly invasive. It is characterized by the expression of Vimentin and loss of E-cadherin expression.

MiR-26a and miR-27a were investigated as part of collaboration with Arup Indra, who is interested in the miRNAs' diagnostic, on top of therapeutic potential to treat melanoma. A study introduces the role of miR-26a in breast cancer as a tumor suppressor by acting on various carcinogenesis-related processes. MiR-26a mainly impacts migration of breast cancer cells and their proliferation.[7] Another study demonstrates how miR-27a promotes breast cancer through angiogenesis and by managing endothelial differentiation of breast cancer stem-like cells.[8]

Current models of biosensors include dual-molecular beacons, molecular beacons, intercalator biosensors, dual linear probes, molecular sentinels, NanoFlares, and double-strand displacement biosensors. The general advantages for some of these biosensors include: high sensitivity and selectivity. However, some may also suffer from a lack of high selectivity, low sensitivity, slow analysis, or false signals. False signals shrink the imaging contrast for cellular analysis in addition to the detection sensitivity. Oligonucleotide-based fluorescent biosensors for *in situ* analyses are complicated by degradation of the sensor from nucleases. These nucleases are capable of cleaving off the quencher or fluorophores on the oligonucleotide biosensor, leading to false signals. While current forms of biosensors have the ability to detect large amounts of miRNA, they fail to measure small changes and low levels of miRNA expression. The problem with current biosensors is the false signals bury the signal from miRNA detection in the baseline signal. It is essential to develop a biosensor capable of measuring small changes in miRNA because early detection requires measurement of femtomolar to nanomolar levels of miRNA. Selectivity of the biosensor is also important because miRNA sequences can differ in the slightest bit (Such as, a difference in three nucleotides). A biosensor able to discern these minimal amounts and miniscule sequence changes will prove to be beneficial towards the detection of early disease and cancer progressions.[5]

In the reporter-probe biosensor design presented in this paper, two dyes located on opposing ends of the reporter are forced into near proximity. Forcing the near proximity interaction not only helps decrease false signal errors, but also encourages fluorescence resonance energy transfer (FRET)—essentially an energy transfer between fluorophores.[9] During the incidence of FRET, only the donor fluorophore is excited by

electromagnetic radiation conducted at a wavelength unique to the donor, but not the acceptor. In this way, the donor is selectively excited. The donor can then non-radiatively transfer its excitation energy to the acceptor fluorophore that will subsequently emit at a new wavelength specific to the acceptor. Two key criteria must be satisfied for this to occur: proximity and compatibility.[10] In order for FRET enhancement to occur, the distance between the fluorophores should be within 1-10 nm of each other. Conversely, if both dyes are too close—within 1 nm of each other—quenching can happen as a consequence.[5] Quenching is when the excited state of the molecule finds an alternative non-radiative path to the ground state, for example as heat rather than light. Quencher molecules that are chemically related to fluorophores have this property.[10] In terms of compatibility, the emission energy (wavelength) of the donor must overlap with the excitation energy of the acceptor. In addition, the molecules must be accurately oriented to maximize energy transfer.

Figure 1: Visual of experimental set up. Acronyms defined: Laser= Mai Tai, M1= Mirror #1, M2= Mirror #2, BS= Beam Sampler, PD= Photo diode, LP-DM= 705 nm Long-Pass Dichroic Mirror, L= 25 mm Focal Length Lens, CH= Cuvette Holder, SPF= 720 nm Short-Pass Filter, Obj= Objective (10x, 0.25 NA), FC= Fiber Coupler, SM= Spectrometer, PM= Power Meter and CPU= Central Processing Unit. [6]

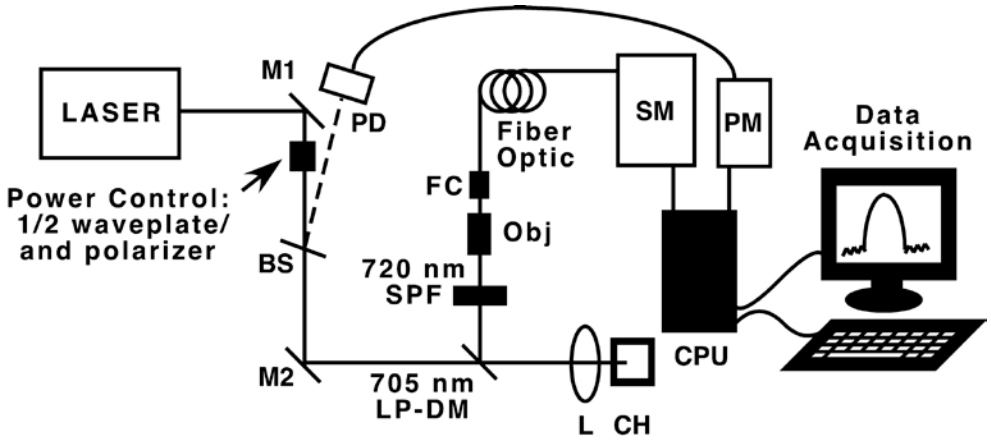

Figure 1, referenced from Larkey, et al., 2014 is a visual of the experimental set up of the custom-built fluorimeter used to run numerous experiments in the Burrows Lab, including the following experiments herein. The main components of this custom-built fluorimeter comprise of a Titanium-Sapphire (Mai Tai, Spectra Physics, Newport*)* laser capable of producing 100 femtosecond (fs) long pulses at a rate of 80 MHz. In addition, the Mai Tai laser has a tunable wavelength range spanning from 690 nm to 1040 nm. The wavelength was controlled via the Mai Tai GUI program (Spectra Physics, Newport), and the power of the laser was managed by the rotation of a half-wave plate and Glan-polarizer (Enables controlled-precision of the average power directed towards the sample). The average power was monitored using a beam sampler that reflected about 4 % of the beam to a power meter equipped with a photodiode detector (Newport, 1918-R). In some cases, signal was collected by the Princeton Instruments Acton Spectrometer with an EMCCD camera, and stored in LightField software. For a majority of experiments the QE65 spectrometer was used with Spectra Suite software from Ocean Optics.

Laser light was filtered out using long-pass and short-pass filters so that the signal detected was from the fluorescent dyes. In the following experiments, a 705 nm long-pass dichroic mirror was used to allow any light above 705 nm to be removed from the signal. The dichroic mirror reflects fluorescence signals below 705 nm and directs this light to a 720 short-pass filter. The short-pass filter only allows any light below 720 nm to go through and reach the detector.

The reporter-probe biosensor design used two-photon absorption—absorption of two photons at about twice the wavelength of the single-photon absorption processes—

due to its underlying advantages. Fluorescence occurs at the same wavelength for either single or two-photon absorption. Two-photon techniques use Near Infrared (NIR) light, and inherently restrict the excitation to the focal spot of a lens. These traits give two-photon techniques several advantages such as less photo-bleaching of dyes outside the excitation volume, reduction in cell as well as tissue damage because many bio molecules do not absorb NIR light, but visible light is. Lastly, its restriction of excitation to focal volume and use of NIR light is ideal for future applications in 3-dimentional two-photon cell and tissue imaging[6] because of reduced autofluorescence from cells and tissues, and less scatter from NIR photons. These traits are particularly advantageous for sensitive miRNA detection in addition to imaging because baseline signals will be very low compared to single-photon techniques.

Chapter 1: Validation of Reporter+Probe Biosensor to Detect Low Levels of miRNA and Mitigate False Signals.

Methods

Kinetic and signal stability studies involved gathering signal intensity data at one minute intervals until a total of five minutes had spanned. Data was, acquired every five minutes until a minimum total of thirty minutes had passed. Each minute was a compilation of six replicate measurements with an exposure time of ten seconds. During incubation times and time periods between each measurement, the laser was blocked. This was done to reduce the possibility of photo-bleaching, as well as to help minimize photo-damage to any dyes and oligonucleotides. All data is an average of signal counts that were background corrected (Acquired signal intensity data is subtracted from the initial blank—the buffer—signal).

For the experiments conducted on the behalf of this chapter, we used a Titanium-Sapphire (Mai Tai, Spectra Physics, Newport) laser to excite the dyes. Fluorescence signal collection used either an Ocean Optics QE65 spectrometer for Let-7a or a Princeton Instruments spectrometer for of miR-26a and miR-27a. The instrumentation used to run this experiment was previously described in the introduction section. All data gathered was processed with MATLAB algorithms written by the Burrows lab members.

Chapter 1 Introduction

(Referenced From: Larkey, E. N.; Almlie, C. K.; Tran, V.; Egan, M.; Burrows, M. S. *Anal. Chem.* **2014**, *86*, 1853-1863.)

Figure 1.1 shows how the miRNA will interact with the biosensor to give a signal change. The transformation reaction driving the reporter-probe complex to the probe-target complex and displacement of the reporter is governed by thermodynamics. The design of the reporter-probe complex is to be resistant to nonspecific miRNA binding. However, in the presence of a target miRNA (in this experimental case, Let-7a) the reporter-probe complex is disrupted to form a more thermodynamically stable probe-target complex. This frees the reporter so it will bind to itself, using intramolecular binding, to form a hairpin conformation. Formation of the hairpin forces the donor and acceptor dyes into very close propinquity, causing a change in the signal intensity that can be measured.

Figure 1.1: Schematic of designed biosensor recognition mechanism. Reporter-probe complex contains a non-complementary region near one end of the complex; Target is a miRNA sequence; Lone reporter structure to the right depicts hairpin conformation.

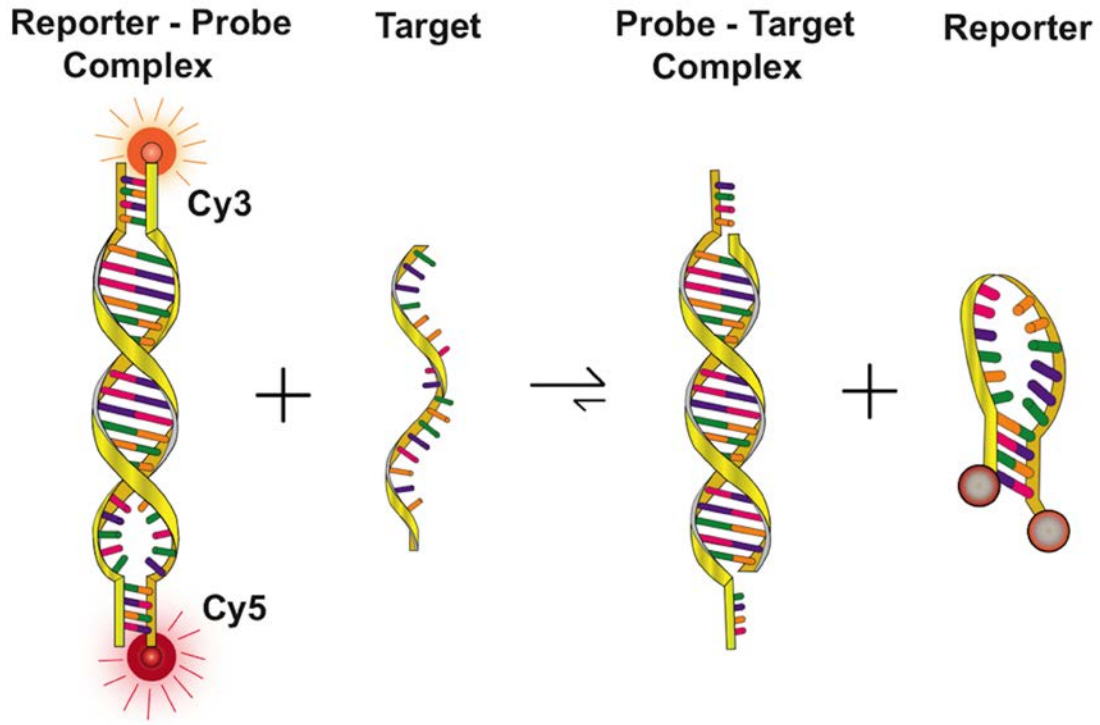

To predict whether this mechanism progresses to the right, a Two State melting (hybridization) application, accessible at the RNA Institute at SUNY-Albany[11] on their DINAMelt Web Server, was used to obtain Gibb energy values. Gibbs is an energy metric that determines if a reaction will proceed naturally. Gibbs energy must be negative for a reaction to proceed naturally. For instance, if the reaction in Figure 1.1 has a negative Gibbs energy, then the probe-target complex and reporter hairpin will form. If the Gibbs was positive, then the reporter-probe complex would remain intact and no probe-target would form. The larger the value of negative Gibbs energy is, the more the reaction in figure 1.1 is inclined to produce end products of a single hairpin reporter and a probe-target complex.

Two types of probes were tested: probe1 and probe2. Probe1 is a specific design where there was only partial complementarity to the reporter's loop region, whereas probe2 had stems that were fully complementarity to the reporter stems. Probe2 maintained the same non-complementary region with the reporter as probe1. In other words, probe1 did not bind to the stems of the reporter, but probe2 did. The purpose of probe2 was to compare false signal to probe1. Nonetheless, it is also important to note both reporters were designed to be fully compatible to Let-7a.

Results from predicted Gibbs binding energy found the reaction of reporter (R) plus probe (P) to form reporter-probe (RP) was -13.1 kcal/mol for probe1 and -19.5 kcal/mol for probe2. In comparison, the respective corresponding reactions of RP plus miRNA target (miR) gave more negative Gibbs values. Probe1-target had a Gibbs binding energy of -23.0 kcal/mol, and probe2-target had -24.7 kcal/mol. Since R + P = RP has a negative Gibbs value and because the Gibbs of RP + miR = (P + miR) + R is more negative than that of RP, the reaction was predicted to proceed from R to RP to (P + miR). The larger negative Gibbs energy values indicate that, indeed, the probe-target complexes are thermodynamically favorable compared to their reporter-probe counterparts.

Figure 1.2: Fluorescence emission of reporter-probe with Cy5 and Cy3 fluorophores, excited with approximately 100 mW at 742 nm. Part (a) shows Cy5 emission range of 620 nm to 690 nm. Part (b) is Cy3 emission from 540 nm to 590 nm. Blue line indicates a 1 µM reporter; green dashed line indicates a 1 µM reporter-probe1 complex; red dashed-and-dotted line means 1 µM reporter-probe1 + 1 µM target.

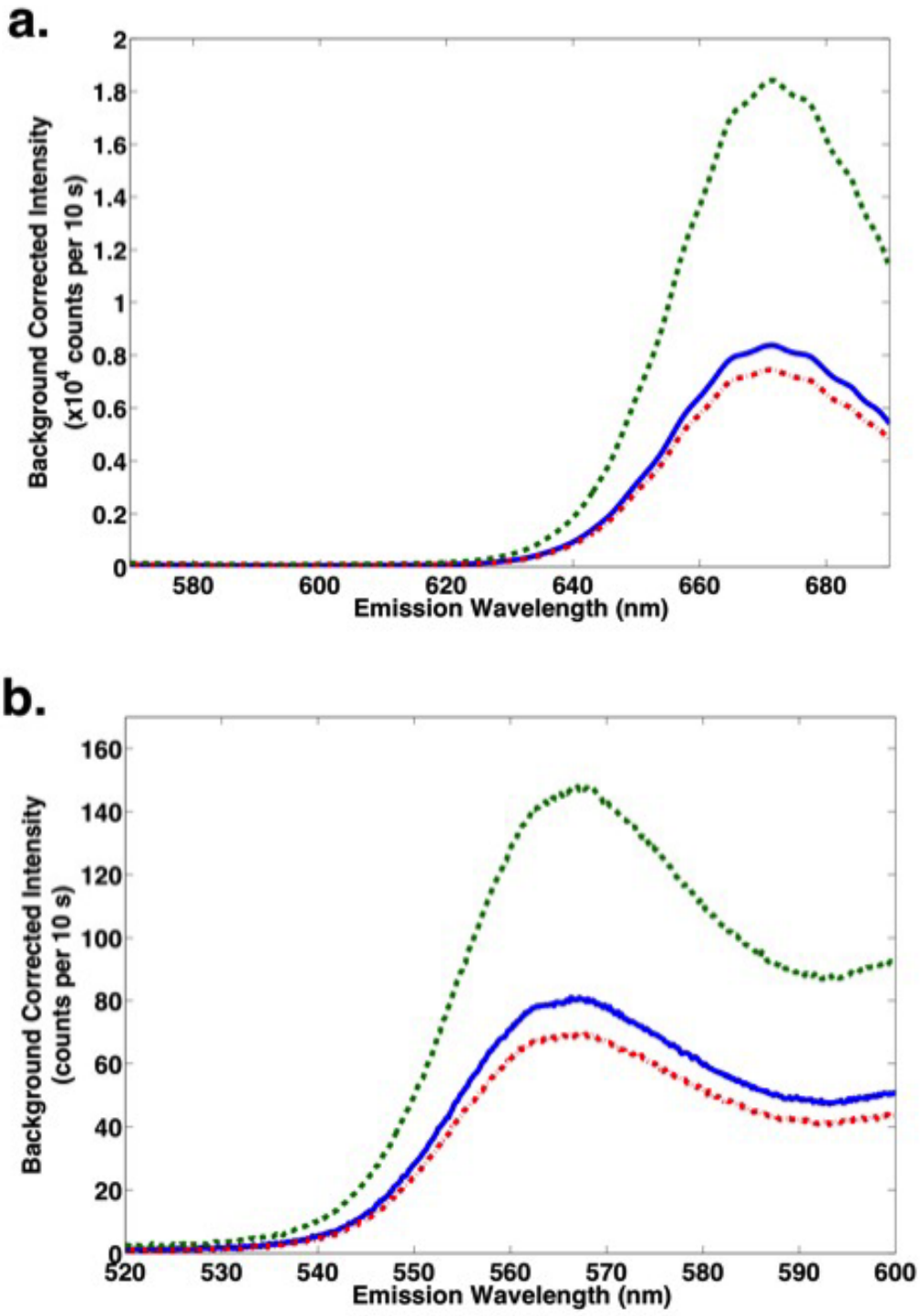

To ensure these reporter-probe sensors can detect miRNA, an experiment testing the signal change was conducted to determine if our observations would match our thermodynamic predictions. Figure 1.2 summarizes the fluorescence emission findings from the transduction mechanism of the reporter-probe1 biosensor with Cy5 and Cy3 fluorophores attached to the ends of the oligonucleotide strand. The reporter was excited at 742 nm with about 100 mW of average power. Results from the Cy5 reporter in the hairpin configuration (1 µM), demonstrated an initial count of 8000 per 10 seconds at an emission of 670 nm, (Figure 1.2a, blue line). Addition of 1 µM probe1 to the 1 µM reporter resulted in an increase in Cy5 signal to roughly 18,000 counts per 10 seconds (Figure 1.2a, green dashed line). Conformation of miRNA biosensing was demonstrated as the signal count returned to approximately 7,000 counts (Figure 1.2a, red dashed-and-dotted line) indicative of the hairpin structure when 1 µM Let-7a was combined with 1 µM reporter- probe1.

In comparison, the Cy3 emission from the reporter hairpin produced a signal intensity of about 80 counts (Figure 1.2b, blue line). With the addition of 1 µM probe, the signal count increased by about 57 %, with a value of approximately 152 counts (Figure 1.2b, green dashed line)—following the trend of the reporters Cy5 signals: an increase in counts. The Cy3 signal also reduced back near the original value (70 counts) when 1 µM Let-7a was added to 1 µM reporter-probe1 (Figure 1.2b, red dashed-and-dotted line). Although the addition of probe to the reporter augmented a bigger signal count, the signal change from Cy3 paled in comparison to Cy5—100 counts per 10 seconds and 10,000 counts per second, respectively. Meaning, Cy5 emission can be considered the more dominant contributor to the reporter's analytical signal.

The biosensor was originally designed with Cy3 and Cy5 in an attempt to create a signal-on type biosensor. Signal-on refers to starting from essentially no signal to having lots of signal. On the contrary, a signal-off sensor represents the opposite: beginning with high signal, and with the addition of miRNA analyte, lowers the signal intensity. Our observations discovered the biosensor functions as a signal-off type; rather than signal-on. Although our reporter is not a signal-on type biosensor, this discovery can be beneficial. Some disease-related miRNA, like Let-7a, are actually down-regulated (I.e., Loss of expression), and, as a result, is underexpressed in cancers and diseases. Recall this is the case when oncogenes will be overexpressed because the miRNA is downregulated. Therefore, there is a need for a fresh cancer diagnostic tool that is capable of detecting the absence of miRNA, rather than its presence. Having a signal-off biosensor is ideal for this scenario because when miRNA, like Let-7a, are absent, the biosensor will be on, whereas when Let-7a is present, the sensor will be off or at a reduced level.

The data introduced also showed quenching of the Cy5 when the reporter was in the hairpin conformation. Ideally, the blue line and the green line should be switched if, indeed, there was fluorescence resonance energy transfer that enhanced the Cy5 signal. However, our observations made evident there is some form of quenching occurring in the hairpin conformation. Ongoing investigations are being conducted in the Burrows lab to learn what type of quenching occurs.

Figure 1.3: Bar graph assessment of percent change in signal due to nuclease degradation in reporter-probe biosensors, and other current models of biosensors (i.e., Molecular beacon technology and double-strand displacement biosensors).

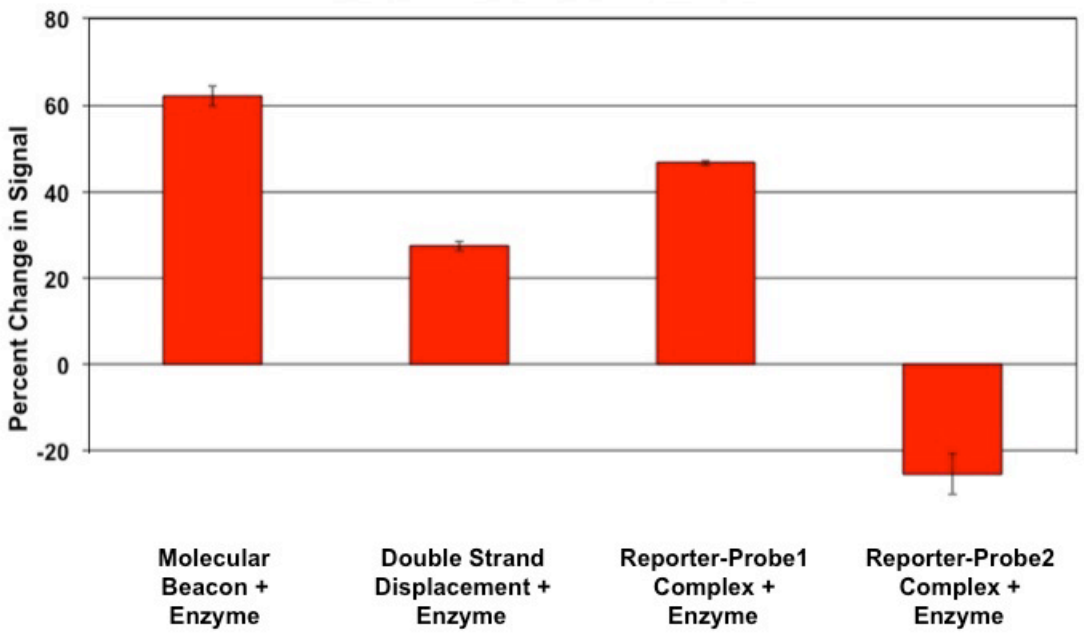

To further investigate the biological potential of the reporter-probe biosensor, we investigated the extent of false signals with respect to conventional biosensors. Figure 1.3 is a summary of our findings. These biosensors, not only demonstrated selectivity, they exhibited a decrease in false signal from endonuclease degradation, a significant issue facing various oligonucleotide-based biosensors today. Molecular beacons, double-strand displacement biosensors, as well as reporter-probe biosensors were exposed to nucleases and the change of signal was measured. Mathematical equations (Equations not shown) were used to calculate the percent change in signal attributable to enzyme degradation. The molecular beacon displayed a percent difference of 62 ± 2 %, while the double-strand displacement showed a 27 ± 1 % change in signal. The reporter-probe1 complex showed 47 ± 1 % change in signal, signifying there was a reduction in false positives.

However, due to the endonuclease's inability to fully digest the stems within the reporter, the stems were able to find each other and rebind, causing a false change in the signal. Therefore, reporter-probe1 has a higher reported false positive error compared to the double-strand displacement biosensor. To address this error, reporter-probe2 was made to have the probe stems bound to the reporter stems, to compel the endonuclease to degrade those regions too. As a result from this change, an observed percent change in signal was: -25 ± 5 %. Reporter-probe2 biosensor expressed no false positives; rather, the negative percent change represents a false negative. Though, the degree of which the false negative extends to is similar to the value of the double-strand displacement biosensor's false positives. Thus, proving how our biosensors are nearly on par with current biosensors, but in some ways, better than some biosensors in the fact that they do reduce false positives. The false negative was due to quenching of Cy5 from the nucleic acids. Plans are in place to keep one reporter-probe stem but leave the other stem open.

Results

Table 1.1: Table of reporter, probe1, Let-7a target, Let-7a variant, miR9 sequences. Bold= complementary binding sites; += location of locked nucleic acid; *= location of a phosphorothioated modification; (m)= location of a 2′O-methyl modification.[5]

Name	Sequence from 5-prime end to 3-prime end
Reporter	Cy5/CATCGTTGAATAC+**TAGGTTGT+ATAGT**TCGAT+G/Cy3Sp
Probe1	**ACTATACAACCTACTACCTC**
Let-7a target	**U*GA*GGmUAmGUAGGUUmGUmAU*AGU*U**
Let-7a variant	**U*GA*_u_GUA_ca_AGGUUGUAU*AGU*U**
miR9 Nonsense	U*CA*UAmCAmGCUAGAUmAAmCC*AAA*GA

Figure 1.4: Evaluation of the selectivity, stability, and biological potential in cell lysate of reporter-probe1 biosensor for Let-7a. Biosensor was exposed to Let-7a, Let-7a variant (Let7aV) and miR9 in buffer. Selectivity was evaluated as percent decrease in signal. Parameters of evaluation consisted of replicate measurements N=3 ("*"= "N=6" and stability study) with an exposure time of 1,000 ms.

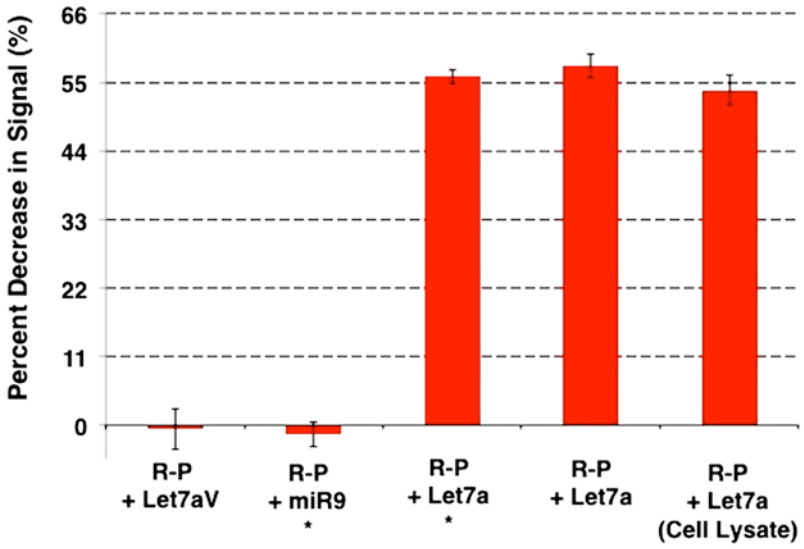

I tested the Cy5 reporter-probe sensor's selectivity towards Let-7a. The biosensor was subjected to variable types of miRNA that were not let-7a, and then closely observed any signal changes. Separate trials consisted of a control with no miRNA added, addition of let-7a, and addition of a Let-7a variant (Almost identical to the original Let-7a sequence, but differing in only three nucleic acids). My graduate mentor, Nick Larkey, also investigated addition of miR9 and addition of Let-7a in cell lysate. Figure 1.4 summarizes the findings of this experiment: The addition of a Let-7a variant to the solution yielded an insignificant modification in signal percentage by -0.6 ± 3.3 %. Putting miR9 in the reporter-probe solution demonstrated a -1.6 ± 2.0 % change. The negative sign indicates that the resulted signal change of the solution actually increased, but those changes were not statistically significant from the value of zero. When compared to the addition of Let-7a in buffer, the percent decrease in signal was roughly

57 %; a much larger decrease than miR9 and the Let-7a variant combined. The addition of Let-7a to the biosensor in cell lysate was investigated to access, if any, the amount of interference from proteins, other RNA species, or DNA to the measurement of Let-7a. The response of the biosensor to Let-7a in cell lysate was about a 53.7 ± 2.4 % decrease in signal. Comparing this value to that in clean buffer (55.8 ± 1.1 %), the percent decrease is not statistically different. The reporter-probe biosensor also demonstrated good stability over a four month time period (55.8 ± 1.1 % at time zero and 57.7 ± 1.9 % at month four). These results demonstrate the biosensor was selective and stable, indicating it has potential for in vivo applications.

Figure 1.5: Bar graph depicting the average background corrected summed intensity of reporter-probe biosensors for either miR-26a or miR-27a with the additions of either analyte or off-analyte.

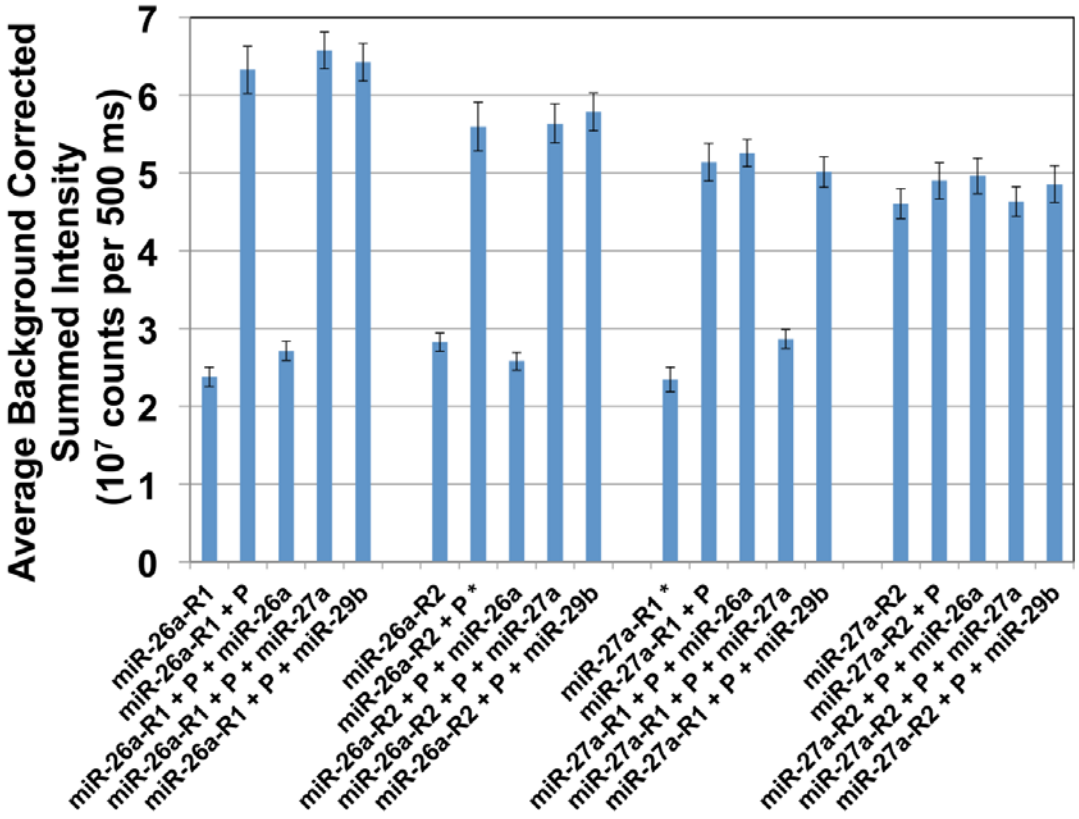

To demonstrate the reporter-probe biosensor works for other miRNA, we designed biosensors for miR-26a and miR-27a. Figure 1.5 goes into more depth as to how these reporter-probe biosensors demonstrate selectivity similar to the biosensor for Let-7a. MiR-26a-R1 alone produces a distinct measurable analytical signal of approximately 2.4 x 10^7 counts per 500 ms. When presented with the probe, the intensity shot up to about 6.3 x 10^7 counts per 500 ms. The signal intensity returns to near the original level (Similar to when the reporter was alone) once the target miR-26a was included—2.6 x 10^7 counts per 500 ms. Additions of off-analytes: miR-27a and miR-29b, did not significantly change the signal from the reporter-probe's value for both miR-26a-R1 and miR-26a-R2. MiR-26a-R2 alone produced about 2.8 x 10^7 counts per 500 ms. Incorporating probe increased the counts to around 5.5 x 10^7 per 500 ms. The addition of miR-26a returned the counts back to the "original" value.

Examination of the biosensors for miR-27a revealed only the miR-27a-R1 to be functional and miR-27a-R2 did not work very well. MiR-27a-R1 unaccompanied had a signal intensity count of 2.3 x 10^7 per 500 ms. Introducing probe brought the count higher to about 5.1 x 10^7 per 500 ms. Then, the count fell back to a similar range as reporter alone with counts of (2.9 x 10^7 per 500 ms) after presenting miR-27a (the analyte). Additions of off-analytes miR-26a and miR-29b gave 5.2 x 10^7 counts per 500 ms and 5.0 x 10^7 counts, respectively. MiR-27a-R2 had comparable results from addition of probe, miR-26a, miR-29b, and miR-27a. The reason for miR-27a-R2 lack of signal change is currently under investigation in the Burrows lab. They are finding it has to do with a possible stable reporter homodomer or open non-ideal hairpins.

Despite which reporter-probe was being analyzed, all reporters demonstrated the same pattern: whenever the target miRNA analyte—e.g., miR-26a or miR-27a—, was introduced, the count intensity would return to nearly the original levels similar to that of the lone reporter. However, any time an off-analyte was incorporated, the signal count remained quite high and within the range of the count level of reporter-probe. This pattern demonstrates selectivity in the biosensors because the designed reporter-probe will only bind to the analyte. Moreover, these findings pursue the same results found when testing the reporter-probe biosensor mechanism for Let-7a. As a refresher, the reporter signal intensity seems to occur at a lower intensity than the reporter plus probe, and returning to nearly the reporter intensity when target was added to the reporter-probe complex. In some cases the signal from the reporter-probe plus target would be about 10 % larger than the reporter alone. The reason for this is still under investigation but could be due to incomplete probe binding to reporter prior to target addition.

It is important in breast cancer diagnostics to detect the concentration of miRNA. The sensitivity of the biosensor was confirmed by analyzing the sensor's capability of detecting low concentrations of Let-7a, miR-26a, and miR-27a. Observations revealed concentrations were detected down to the nanomolar level by using the reporter-probe biosensors. Utilizing the biosensor concentrations of 1 μM and 100nM, the limits of detection, limits of quantitation, and sensitivity were determined from calibration studies (Data not shown). The "limit of detection" is how small of a concentration that can be detected, whereas "quantitation limit" is defined as how low of a concentration can be quantified. Studies indicate the 1 μM reporter-probe1 biosensor has a detection limit of 9 ± 4 nM as well as a quantitation limit of 18 ± 4 nM. A 100 nM reporter-probe1 complex

yielded a detection limit of 4 ± 1 nM, and a quantitation limitation of 16 ± 2 nM. Formerly, the tested sensitivity of the 1 µM sensor displayed an approximate count of 9.5 x 10^4 per nM. By increasing the exposure time for 100 nM reporter-probe1 biosensors to 500 ms, the sensitivity counts changed to 3.6 x 10^4 per nM.

Table 1.2: Analytical figures of merit for 100 nM reporter-probe biosensors.

	Lethal- 7a	miR-26a*	miR-27a	N
Detection Limit (nM)	4 (± 1)	1.80 (± 0.78)	2.58 (± 0.38)	**3**
Quantitation Limit (nM)	16 (± 2)	6.00 (± 2.60)	8.60 (± 1.27)	**3**
Sensitivity (counts/nM)	-3 x 10^5	-5.95 x 10^{-3}	-3.60 x 10^{-3}	**3**
Linear Dynamic Range (nM)	4 - 100	1.80 - 100	2.58 - 100	**3**

(*) = Indicates N=6

Table 1.3: Reporter-probe complex calibration curve slopes of miR-26a, and miR-27 with 100 nM analyte and without 100 nM off-analytes. N= number of calibration curve experiments conducted. (*)

	Average Slope ± RSD	**N**
miR-26a-R1	$-5.95 \times 10^{-3} \pm 5.14$ %	6
miR-26a-R1 + Off Analytes	$-5.84 \times 10^{-3} \pm 5.58$ %	3
miR-26a-R2	$-6.24 \times 10^{-3} \pm$ 13.68 %	3
R-26a-R2 + Off Analytes	$-5.88 \times 10^{-3} \pm 4.49$ %	3
miR27a-R1	$-3.60 \times 10^{-3} \pm$ 18.55 %	3
miR27a-R1 + Off Analytes	$-3.79 \times 10^{-3} \pm$ 15.99 %	3

Tying in this concept with the previously mentioned calibration curve slopes, the prediction suggests that because they have similar counts, they would also display similar slopes, which was what was discovered.

Table 1.3 illustrates the sensitivity from the calibration curves of our biosensors (Calibration curves not shown). MiR-26a-R1 had an average slope range of $-5.95 \times 10^{-3} \pm 5.14$ %. When off-analytes were added to miR-26a-R1, the average slope was found to be $-5.84 \times 10^{-3} \pm 5.58$ %. The two slopes are not statistically different, thus can be deemed identical. MiR-26a-R2 also follows this same trend: miR-26a-R2 had a calibration slope of $-6.24 \times 10^{-3} \pm 13.68$ %, while miR-26a-R2 with the addition of off-analytes exhibited a slope of $-5.88 \times 10^{-3} \pm 4.49$ %. Hence, it is not as surprising to find that miR27a-R1 had the same pattern with a slope of $-3.60 \times 10^{-3} \pm 18.55$ %, and miR27a-R1 plus off-analyte had a slope of $-3.79 \times 10^{-3} \pm 15.99$ %. The fact the calibration curve slopes with and without off-analyte were very similar, demonstrates fantastic selectivity of the biosensor.

Chapter 1 Conclusion*:*

Reporter-probe biosensors demonstrate various advantages over current trending models of biosensors (e.g., Molecular beacons, double-strand displacement biosensor, etc.) due to three highlighted key results: (1) An observable reduction in false signals in comparison to various existing models of biosensors by studying percent signal change from nuclease degradation; (2) Its limit of detection on the nanomolar scale and excellent sensitivity *(*10^5 counts/nM); (3) Lastly, its high selectivity, seen when the signal is turned off while the reporter is in a solution consisting of probe and analyte, and when signal is on when off-analyte is present. All findings contribute to the design of optimal biosensors that are highly sensitive, have negligible false positive errors, as well as possess great selectivity for accurate results. Biosensors can then be applied in breast cancer diagnostics for improved early detection of the disease, allowing humanity to take down the cancerous-biomolecules before the cancer is even able to strike.

Not to mention, throughout experimentation, we discovered our biosensor is a signal-off type sensor, which is great for measuring the absence of miRNA similar to Let-7a that regulates oncogenes. On the down side, signal-off type sensors are not ideal for measuring miRNA regulating tumor suppressor genes because that population of miRNA will be over-expressed in cancers. Therefore, signal-on sensors are still in demand. Our lab group has recently published work in Analytical Methods demonstrating signal-on and signal-off sensors are comparable rather than competitive as ideal sensors.

Chapter 2: Investigation of Two-Photon FRET Pairs and use of Carbon-Oxygen spacers for Signal Enhancement using Linear Strands of DNA

2.1 FRET pair studies on linear DNA strands

Methods

Various Fluorescence Resonance Energy Transfer (FRET) donor and acceptor pairs were investigated for their ability to enhance the fluorescence signal by energy-transfer mechanisms. Excitation wavelengths from 742 nm to 1032 nm in 10 nm steps were investigated. The dyes studied were Alexa Fluor 488, Alexa Fluor 532, Cy5, Atto 633, Alexa Fluor 594, Atto 590, Alexa Fluor 546, and Cy3. Table 1. Lists the linear single strands of oligonucleotide deoxyribonucleic acids (DNA) that were attached with varying dyes on one end.

Table 2.1: Dyes, Oligonucleotide sequence, and dye placement on oligonucleotide.

Name*	Sequence (5′ to 3′)
5pAlex488	Alexa Fluor 488 / TGAGGTAGTAGGTTGTATAGTT
5pAlex532	Alexa Fluor 532 / TGAGGTAGTAGGTTGTATAGTT
5pCy5	Cy5 / TGAGGTAGTAGGTTGTATAGTT
3pAlex546	AACTATACAACCTACTACCTCA / Alexa Fluor 546
3pCy3	AACTATACAACCTACTACCTCA / Cy3
3pAtto590	AACTATACAACCTACTACCTCA / Atto 590
3pAlex594	AACTATACAACCTACTACCTCA / Alexa Fluor594
3pAtto633	AACTATACAACCTACTACCTCA / Atto 633

* 5p = 5-prime (5′) end of oligonucleotide, 3p = 3-prime (3′) end of oligonucleotide. All 5-prime reporter strands are complementary to the 3-prime reporter.

Samples were prepared under hood to keep solutions sterilized and protected from miRNA degrading enzymes. From the stock solutions of the reporters (Varied in concentrations), we made diluted samples of 1µM solutions for the experiment. Then, combinations of dye pairs on complementary strands of DNA were allowed to hybridize to form a complex called a heterodimer. Table 2.2 demonstrates the investigation of various dye-pair heterodimer combinations. Figure 2.1 shows the hybridization reaction for the ideal situation where donor dye signal decreases as acceptors signal increases due to energy transfer between the dyes. However, we discovered it was a common occurrence among the heterodimers in which both signals from the dyes were quenched.

Figure 2.1: Shows the hybridization reaction for the FRET studies. In the ideal case the donor (D) emission will decrease and acceptors (A) will increase after hybridization. Often both dyes exhibited quenching instead of the ideal scenario. The arrowhead represents the 3-prime (3′) end and the arrow tail represents the 5-prime (5′) end of the DNA strand. The cartoon does not properly portray that the 5′Cy5 was actually the acceptor when hybridized with 3′dye pairs.

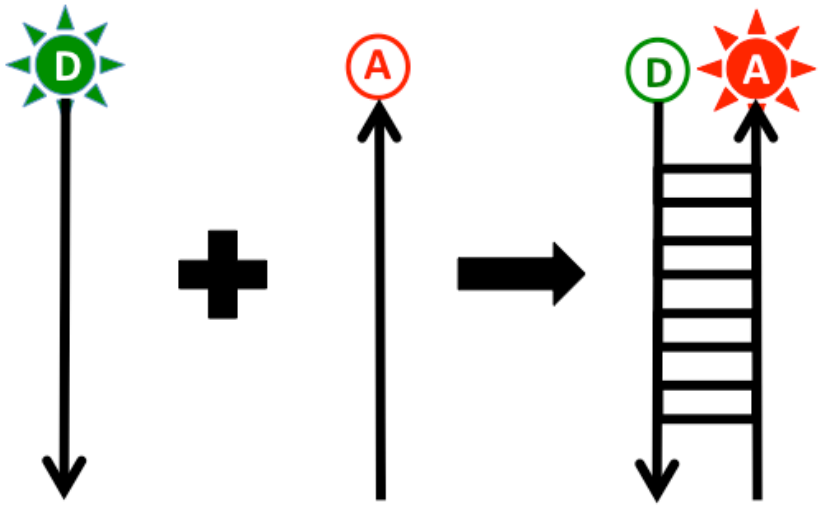

Table 2.2: Dye-pair combinations investigated.

	3pAtto633	**3pAlex594**	**3pAlex590**	**3pAlex546**	**3pCy3**
5pAlex488	X, E	X, E	X	X, E	X
5pAlex532	X, E	X	X	X	X
5pCy5	X	X	X	X	X, E

* E = enhancement observed

Each dye-labeled single-strand was individually excited at different wavelengths and the emission was measured to obtain the baseline signal for each dye. This was done to establish a reference point to determine if the signal changes by either quenching or enhancement upon hybridization to a complementary strand with a different dye. For each dye-pair investigated, the contribution of signal from each dye alone was summed to allow us to generate emission spectra that simulated baseline signal intensity as if the two dyes were on a hairpin structure. Burrows members processed the collected data through a pre-designed MATLAB code in order to generate excitation and emission spectra to subsequently determine enhancement, quenching, percent changes, and energy transfer efficiency.

Percent Change (%ΔF) in signal was calculated using the intensity over an emission region of the spectrum, $\Delta\lambda_{\text{Acceptor}}$, where the acceptor emission dominates, $F(\Delta\lambda_{Acceptor})$. However, to gauge any contribution from the donor emission in the acceptor's emission region, we summed the donor and acceptor intensity in the acceptor's emission region of interest. A ratio of emission from the FRET pair and the acceptor alone plus donor alone was calculated using the following equation:

$$\%\Delta F = 100\ x\ \left(\frac{F(\Delta\lambda_{Acceptor})_{FRETpair}}{F(\Delta\lambda_{Acceptor})_{Acceptor\ Alone} + F(\Delta\lambda_{Acceptor})_{Donor\ Alone}} - 1\right)$$

A custom built fluorimeter was used to excite and collect emission from the samples and was previously described.[5] Briefly a Mai Tai HP (Spectra Physics) laser was used to excite the samples and tune the excitation wavelength from 742 nm to 1032 nm in 10 nm steps. The peak width of the excitation band was about 15 nm. Power was controlled using a quarter waveplate and polarizing beam splitter. Power was adjusted at each wavelength to ensure an average power of 100 mW reached the sample. Each emission spectra was obtained by exposing the CCD camera in the QE65 for 1,000 ms, 10 scans of spectra were collected 4 times. This was done to reduce noise and have a measure for instrumental error.

Section 2.1 Results

Out of the pairings studied, Figure 2.3 reveals that only a few showed FRET enhancements when excited in the 892 nm to 1022 nm region. Beginning with 5′Alex 488 when paired with 3′Atto 633, a remarkably large signal increase was observed, about 366.81 %, when excited at 922 nm. The pair with 3′Alex594 only gave an 11.59 % signal increase when excited at 932 nm. The least enhancement observed was with the 3′Alex 546 pair that gave approximately 2.67 % signal increase when excited with 912 nm. On the other hand, pairs with 3′Cy3 and 3′Atto 590 only exhibited quenching over the entire excitation range from 740 – 1040 nm.

Figure 2.2: Percent change in signal as a function of excitation wavelength for 5′Alex488, 5′Alex532, and 5′Cy5 paired with various potential FRET dyes.

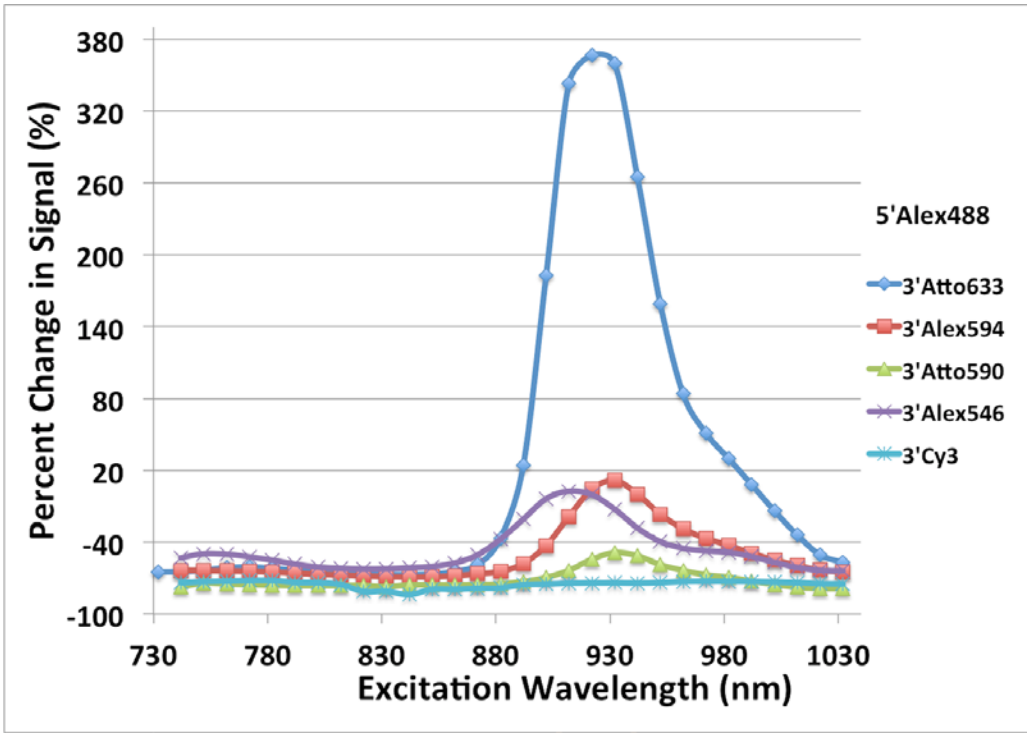

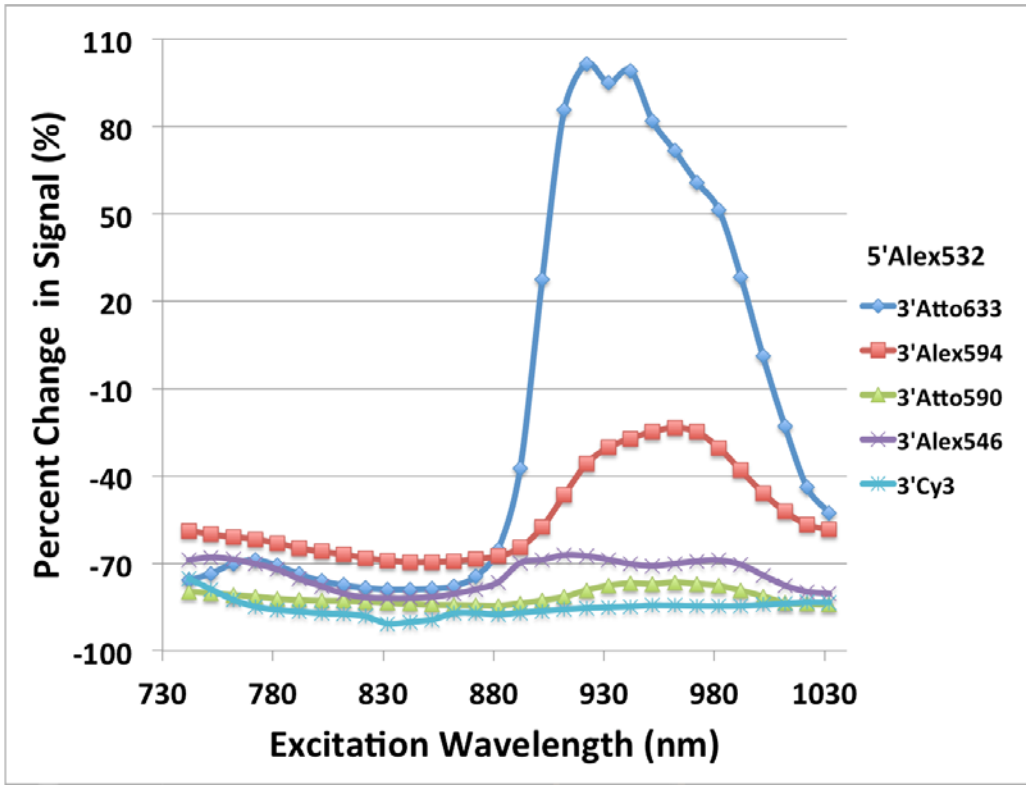

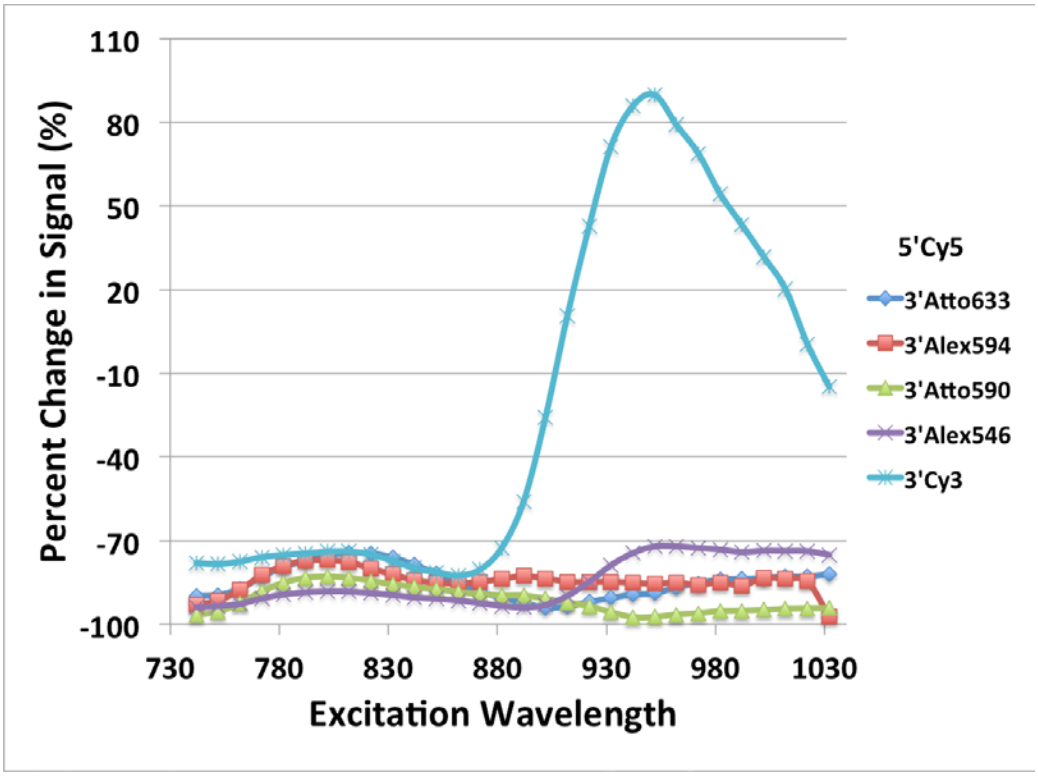

In comparison, 5′Alex532 exhibited enhancement with just the 3′Atto633, whereas the other four pairs resulted in quenching. When 5′Alex532 was bound to 3′Atto633, about a 101.65 % signal increase occurred when excited with 922 nm. However, when bound with 3′Alex 546, 3′Alex 594, 3′Atto 590, or 3′Cy3, quenching is seen over the entire excitation wavelength range studied. Similarly, the 5′Cy5 showed enhancement with just one dye, the 3′Cy3. For this pair, the signal was enhanced by about 89.84 % when excited at 952 nm. Yet, when paired with either 3′Alex 546, 3′Alex 594, 3′Atto 590, or 3′Atto 633, the result was quenching over the entire excitation wavelength regions studied.

Table 2.3: Strongest and weakest quenching at associated excitation wavelength for each dye-pair studied

Dye Pairs	Strongest Quenching	Weakest Quenching
5′Alex488-3′Atto633	–66.99 % (842 nm excitation)	–13.82 % (1002 nm excitation)
5′Alex488-3′Alex594	–69.07 % (842 nm excitation)	–16.71 % (952 nm excitation)
5′Alex488-3′Atto590	–78.76 % (1032 nm excitation)	–48.74 % (932 nm excitation)
5′Alex488-3′Alex546	–63.94 (1032 nm excitation)	–0.31 % (922 nm excitation)
5′Alex488-3′Cy3	–83.75 % (842 nm excitation)	–71.92 % (782 nm excitation)
5′Alex532-3′Atto633	–78.92 (832 nm excitation)	–23.04 % (1012 nm excitation)
5′Alex532-3′Alex594	–69.61 % (842 nm excitation)	–23.43 % (962 nm excitation)
5′Alex532-3′Atto590	–84.50 % (882 nm excitation)	–76.49 % (962 nm excitation)
5′Alex532-3′Alex546	–82.00 % (832 nm excitation)	–67.14 % (912 nm excitation)
5′Alex532-3′Cy3	–90.69 % (832 nm excitation)	–75.26 % (742 nm excitation)
5′Cy5-3′Atto633	–94.02 % (902 nm excitation)	–74.32 % (812 nm excitation)
5′ Cy5-3′Alex594	–97.19 % (1032 nm excitation)	–77.02 % (802 nm excitation)
5′ Cy5-3′Atto590	–97.41 % (942 nm excitation)	–82.80 % (802 nm excitation)
5′ Cy5-3′Alex546	–93.92 % (892 nm excitation)	–71.99 % (962 nm excitation)
5′ Cy5-3′Cy3	–82.49 % (862 nm excitation)	–14.87 % (1032 nm excitation)

Figure 2.2 show each dye-pair of interest had differing patterns of quenching and enhancement at different excitation wavelengths. For instance, when 5′Alex488 was combined with 3′Atto633, the signal change was boosted to an increased enhancement by

366%. The enhancement was varied over the 892 nm to 992 nm, with the weakest enhancement of 8.15 % at 992 nm. Quenching was observed at all other wavelengths for this dye pair. The 5′Alex488-3′Alex594 dye pair only exhibited enhancement over the 922 nm to 942 nm excitation range, with a maximum enhancement of 11.59 %. This dye pair quenched at all the other excitation wavelengths. When 5′Alex488 was partnered with 3′Alex546, signal was only enhanced at 912 nm, 2.67 % signal change, and quenched everywhere else. On the other hand, the 5′Alex488-3′Cy3 demonstrated quenching at all excitation wavelengths. A similar pattern of only quenching occurred when 5′Alex488 was coupled with the 3′Atto 590 dye. Table 2.3 lists the strongest and weakest quenching for all the possible FRET dye-pair combinations.

Looking at dye-pairs for 5′Alex532, enhancement only occurred with 3′Atto633, whereas all the other pairs resulted in quenching. When 5′Alex532 was bound with 3′Atto633, enhancement occurred over the 902 nm to 1002 nm range. The enhancement ranged from 1.13 % to 101.65 % when excited with 1002 nm and 922 nm, respectively. The 5′Alex532-3′Cy3 pair demonstrated the most quenching out of all the 5′Alex532-dye pairs with a - 90.69 % change in signal.

Equally, the dye 5′Cy5 only had one enhancing pair with 3′Cy3, whereas the rest of the dye-pairs resulted in quenching. When 5′Cy5 was paired with 3′Cy3 the signal enhancement occurred over the 912 nm to 1022 nm range, but quenched everywhere else. The 5′Cy5-3′Cy3 enhancement ranged from 0.51 % at 1022 nm to 89.84 % at 952 nm. Table 2.3 reveals that the 5′Cy5-3′Atto590 pair gave a very strong quenching of - 97.41 % at 942 nm excitation. Similarly the heterodimer containing 5′Cy5-3′Alex594 demonstrated - 97.19 % signal change at 1032 nm excitation. Even the 5′Cy5 with

3′Atto633 gave a really strong quenching with a signal change of - 94.02 % when excited at 902 nm. When utilizing a signal-off type biosensor, it is beneficial to have strong quenching of the dyes because it helps to provide a distinct contrast between the signal and the background.

Section 2.1 Discussion

In chapter 1, I discussed development of a reporter-probe biosensor to detect miRNA. The sensor used a self-complementary reporter with a Cy3/Cy5 dye-pair starting in an open conformation when bound to probe. Upon miRNA-probe binding, the reporter is displaced and forms a hairpin structure. The sensor was designed with a Cy3/Cy5 dye-pair in an attempt to achieve Cy5 enhancement by stimulation of Cy3 and subsequent energy transfer to Cy5 when the reporter was in the hairpin conformation. However, our results showed that we received quenching.

In order for FRET to occur the dyes need to be within 1 – 10 nm of each other and they need to have their transition moments well aligned and not perpendicular to each other. If the transition moments are perpendicular, no energy transfer can occur. Furthermore, if the dyes are less than 1 nm apart quenching is observed. We suspect the quenching observed with the biosensor's reporter was due to the dyes being too close, and nucleic acid-based quenching.

The results from chapter 1 on the reporter-probe biosensor lead us to question why the Cy3/Cy5 dye-pair quenched and made us want to explore other potential FRET pairs for use with the biosensor. To this end we used linear strands of DNA to avoid complications of hairpin formation on dye placement.

It was interesting to find, for the dyes tested, all were quenched at 742 nm. Those that generated a signal increase did so between excitation wavelengths of 892 nm to 1022 nm. In fact, all the dyes-pairs showed quenching at various excitation wavelengths. In some cases the acceptor appeared to show enhanced fluorescence, but the contribution from the donor emission would actually mask any enhancement.

Of all the dyes studied the 5′Alex488-3′Atto633 pair gave the best enhancement of 366.81 %. The 5′Cy5-3′Cy3 pair gave the least enhancement compared to 5′Alex488-3′Atto633 and 5′Alex532-3′Atto633. The best quenching observed was the – 97.41 % change in signal with the 5′Cy5-3′Atto590 pair. In general, all the dye pairs of 5′Cy5 gave the strongest quenching.

FRET enhancement was definitely observed over the 892 nm to 1022 nm range depending on the dye-pairs. At various other wavelengths quenching was observed. Without measuring fluorescence lifetimes, it is hard to identify the type of quenching as either FRET based or some other process. We can rule out dynamic quenching and static quenching that arise from either collisions between molecules or formation of a dye-pair complex that renders the molecules non-fluorescent. The reason we can rule these mechanisms out is because we observed enhancement at certain wavelengths for a majority of the dye-pairs studied. Some of the quenching can be attributed to the proximity of the dyes to nucleic acids when the heterodimers form. In fact, the enhancements observed were likely sub-optimal as some of the enhancement was likely lost to nucleic acid quenching.[5]

2.2 FAM/Atto633 FRET Reporter-Probe Biosensor

Section 2.2 Results

From the results in section 2.1 we designed a Fluorescein/Atto633 based biosensor as a signal-on biosensor. The FAM/Atto633 biosensor was designed to meet the need for a signal-on type sensor in addition to the signal-off type biosensor. Fluorescein (FAM) was used for preliminary tests because it is less expensive than Alex488 but has similar spectral properties. We also decided to test one reporter with an 18 atom carbon-oxygen spacer and one without the spacer to investigate potential quenching similar to that observed in the reporter with Cy3/Cy5.

Figure 2.3: Average background corrected summed intensity of R25 excitation spectra with and then without spacers. Graph 1: Blue= “R25FA 0, 011.18.14”; Red= “R25FA 0, 0 + Probe 11.18.14”. Graph 2: Blue= “R25FA 18,18 11.18.14”; Red= “R25FA 18,18 + Probe 11.18.14”

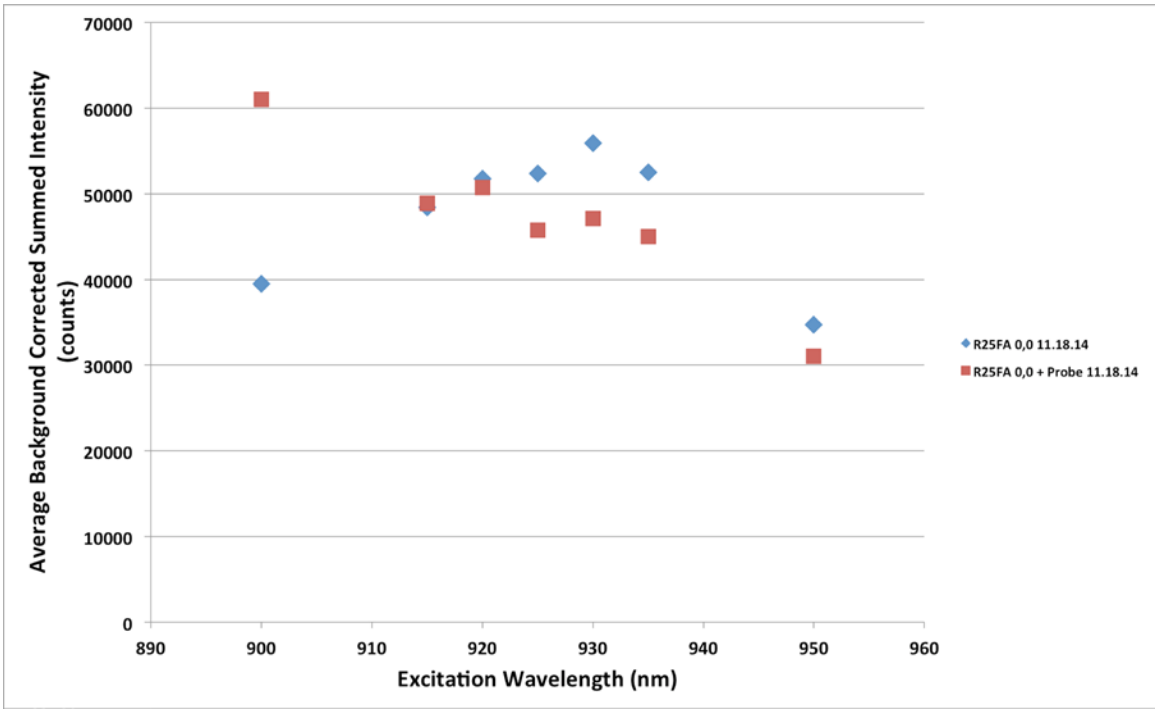

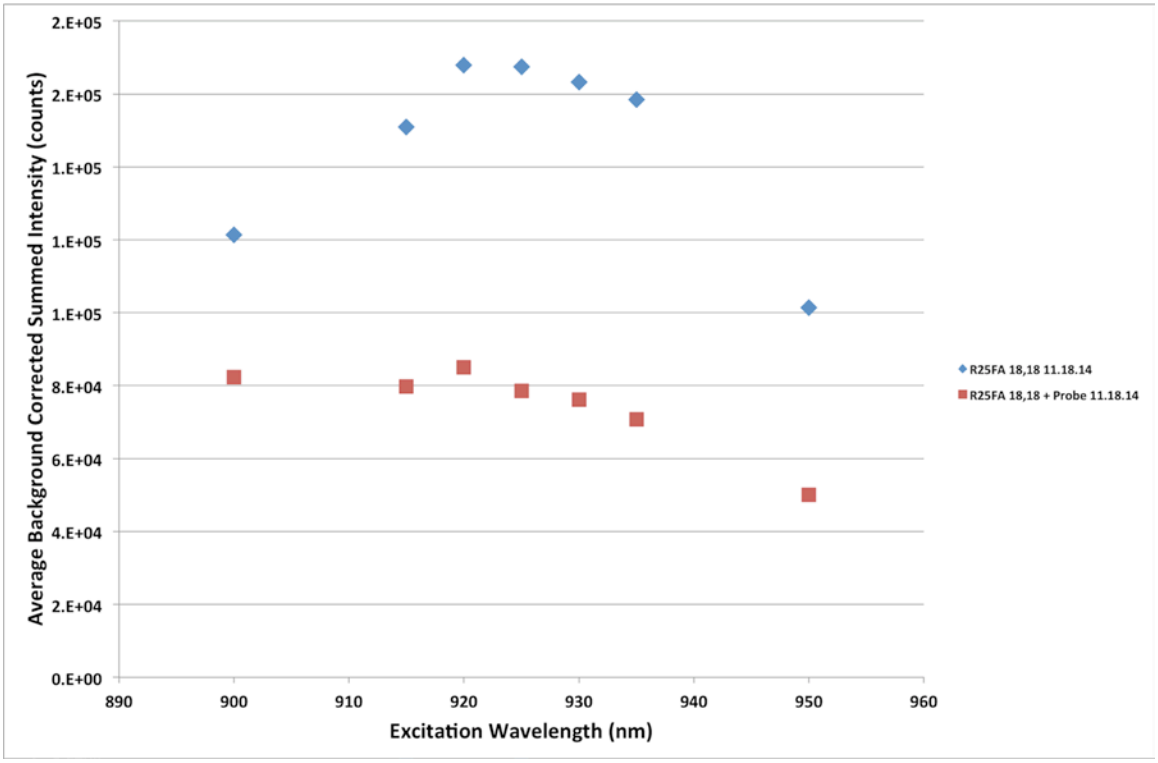

In figure 2.3, the reporter (R25) hairpin without spacers exhibited intensity from Atto633 of approximately 55,000 counts at about 930 nm. Adding probe caused, mainly, a decrease in counts as the excitation wavelength increases. The decrease does signify a FRET signal was present in the hairpin that was disrupted when the probe opened the hairpin. However, the signal change was not very large. When excited at 915 nm and 920 nm there were no discernible differences since the values are near each other. Quenching occurred at an excitation wavelengths of approximately 915 nm. When R25 used 18, 18 carbon-oxygen spacers between the terminal nucleotide and the dye, there was a distinct difference between the reporter hairpin, and the addition of probe. Furthermore, there was no quenching from the selected excitation wavelengths. From this FAM/Atto633 data, we can confirm this biosensor is a signal-on type due to the probe decreased intensity in comparison to the single reporter when probe was added in solution. The data clearly showed the hairpin had FRET.

Figure 2.4: Percent change from R25+P to R25 using FAM and Atto 633.

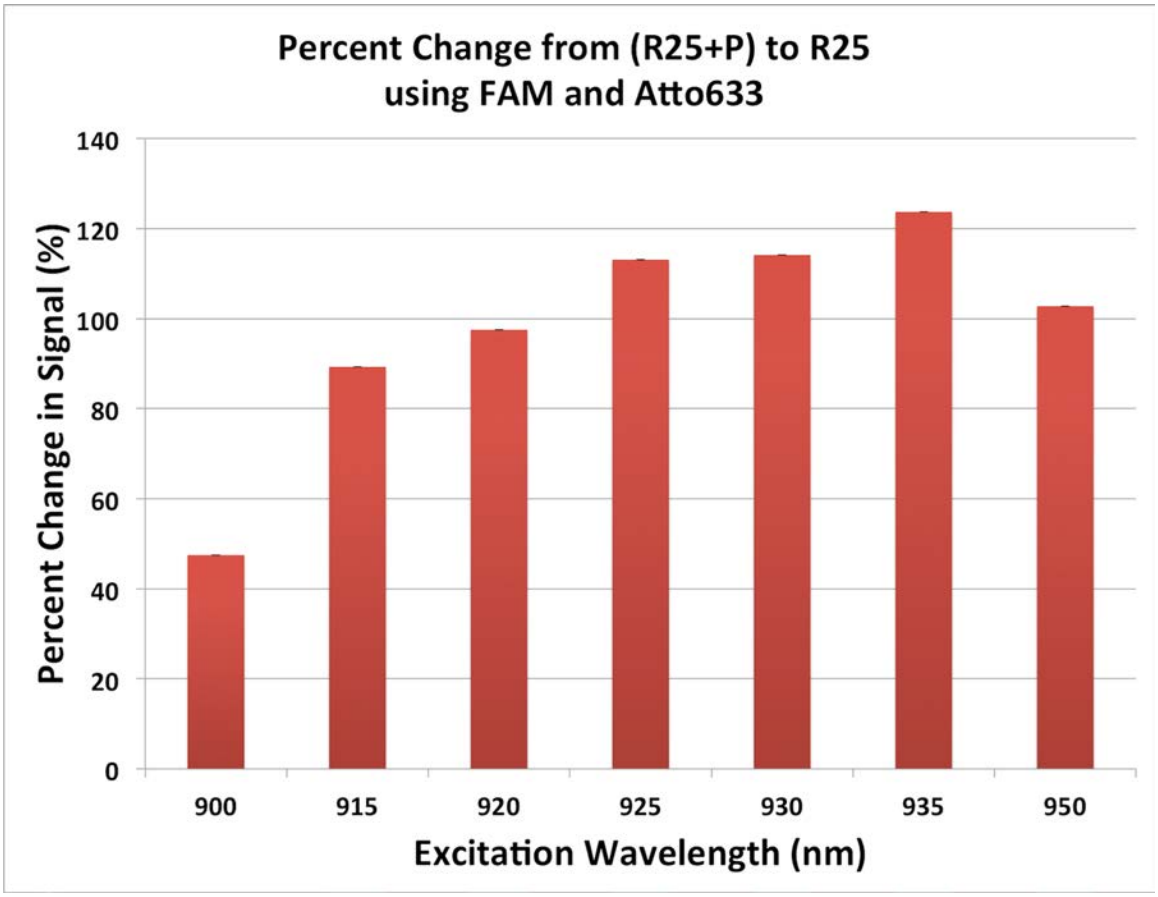

In figure 2.4, the maximum percent change in signal between the FAM/Atto 633 reporter-probe and reporter hairpin was around 935 nm excitation. Previous wavelengths provided a steady increase in percent change. However, at 950 nm, the percent change in signal begins to decline. The work I did to find the FAM/Atto 633 FRET pair and best excitation wavelength allowed Lulu Zhang, a graduate student in the Burrows group, to show nanomolar limits of detection can be achieved with this signal-on biosensor. These results show we are now capable of detecting the presence or absence of miRNA by using either the FAM signal for signal-off or using the Atto633 signal for signal-on.

Section 2.1 & 2.2 Conclusion

The different combination of dyes located at the terminal ends of the strand, do affect certain dye-pairs' energy transferring capabilities. Certain pairs will achieve FRET enhancement or quenching, but were dependent on the excitation wavelength. In this study, we found the 5′Alex 488 with 3′Atto633 pair gave the strongest FRET enhancement, with a grand signal change of approximately 367 % at 922 nm excitation. 5′Alex532 paired with 3′Atto633 follows afterward as second highest signal change at about 102 %. The 5′Cy5-3′Cy3 pair showed the weakest enhancement of about 90 % at 952 nm excitation. When dyes were excited at the wavelength of 742 nm, they all displayed quenching. However, quenching occurred at multiple wavelengths for each dye pair and is tabulated in Table 2.3.

Using my findings from the FRET studies with the linear reporters we ordered a hairpin reporter for the reporter-probe biosensor that had Fluorescein (FAM) and Atto633 on the distal ends. I found that both the FAM/Atto633 reporters with and without the 18 atom carbon-oxygen spacer were capable of FRET enhancement. FRET was evident when observing a decrease in Atto633 emission upon probe addition to the reporter. However, the percent change in signal for the reporter with out the spacer was very small. Promising results with the 18 spacer reporter are showing nanomolar limits of detection.

The findings from this study will be referenced to proceed towards designing and optimizing a working and efficient reporter-probe capable of FRET enhancement, for signal-on applications. Signal-on is ideal for measuring cancer-associated upregulation of a miRNA. However, in some cases cancers downregulate the miRNA, requiring measurement of the absence of miRNA. In such instances, a signal-off, or quenching

based, sensor is desirable. In this case normal cells with the miRNA expressed will be dim, and cancerous cells that have the miRNA downregulated will be very bright. In this case we will want to purse the use of dye-pairs like 5′Cy5-3′Atto590 or 5′Cy5-3′Alex594 that gave nearly 100 % quenching. These reporter-probes can then be used to further study other fields related to application in breast cancer or other miRNA-based disease diagnostics.

3.0 Spacer Studies to Optimize Cy3/Cy5 FRET Efficiency

Methods

Single-strand linear 3′Cy3 and 5′Cy5 reporters with or without carbon-oxygen (CO) spacers were investigated to see if the FRET efficiency between Cy3 and Cy5 could be improved. The nucleic acid sequences for these studies were the same as those used for 3′Cy3 and 5′Cy5 described in section 2 Table 2.1. First, solutions of each reporter alone at 100 nM were analyzed in order to establish a baseline signal as control to determine if either the Cy3 or Cy5 signal changed upon hybridization. Afterwards, hybridized solutions containing the two single-strands were tested (Solutions were hybridized for 30 minutes). Combinations of paired 3′Cy3/5′Cy5 heterodimers with the same or different length carbon-oxygen spacers were investigated to determine quality as well as quantity of FRET enhancement. Table 3.1 depicts the combinations investigated and Figure 3.1 shows a generic hybridization reaction.

Table 3.1: Combinations of paired 3′Cy3 and 5′Cy5 heterodimers.

	3′Cy3-0 spacer	3′Cy3-9 spacer	3′Cy3-18 spacer
5′Cy5-0 spacer	X	X	X
5′Cy5-9 spacer	X	X	X
5′Cy5-18 spacer	X	X	X

Figure 3.1: Generic hybridization reaction for spacer study. The arrowhead represents the 5-prime (5′) end and the arrow tail represents the 3-prime (3′) end. Donor (D) was Cy3 and acceptor (A) was Cy5. The blue line represents a generic carbon-oxygen spacer.

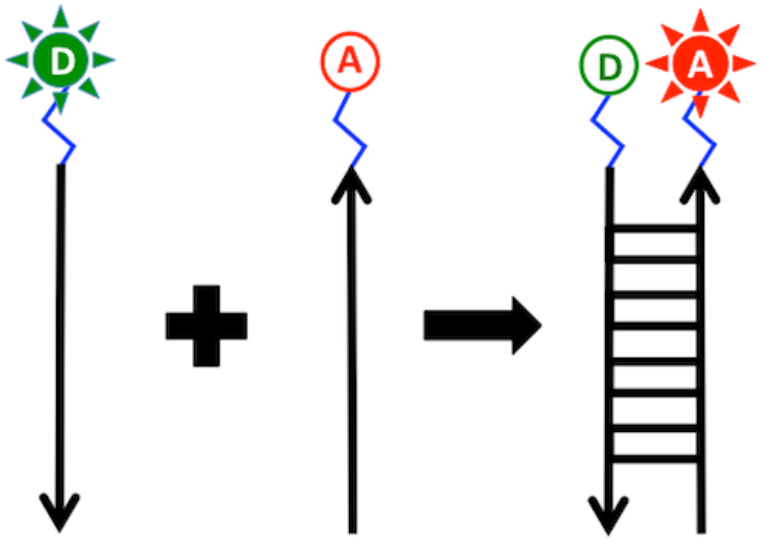

Samples were prepped from an initial solution of typically 1 µM. Solutions of were then diluted with buffer to make 100 nM used for the experiment. The hybridized solution contained 100 nM of each reporter. In this case, 3′Cy3 is the donor and 5′Cy5 is the acceptor.

Figure 3.2: Dilution scheme of sample preparation for spacer studies; preparation for 500 µL of sample.

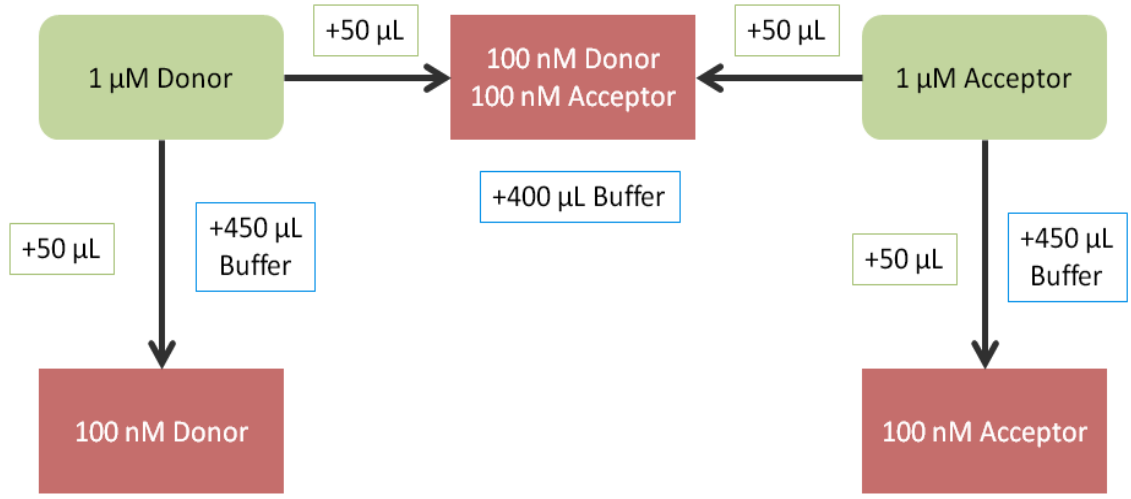

For this study similar parameters from section 2.1 were used again, followed with the same instrumentations: the Mai tai laser, the Princeton Instruments Acton Spectrometer with an EMCCD camera to collect signal, and the LightField Software to store collected data. Samples were excited from 740 nm to 1040 nm in 20 nm intervals, with an excitation power of 75 mW (though, read as 3 mW on power meter). Emission was analyzed using a spectrometer with a 300 groove/mm grating blazed at 500 nm. The center wavelength of the grating ranged from 525 nm to 686 nm, and the entrance port had a slit width of 1,000 µm. Lastly, the mode “step-and-glue” was selected, this allowed for automated movement of the grating center wavelength. The cameras acquisition settings averaged 20 exposures per 500 ms, and 3 cuvette placements to account for cuvette error. The analog conditions were listed as low noise, 100 kHz, and high analog gain. The read out was full frame with the specific region of interest defined as: x= 0, w= 512, and B= 1, then y= 230, h= 68, and B= 4. Where x= pixel number in x-direction, w= width in units of pixels, B= pixel bin size, y= pixel number in y-direction, and h= height

in units of pixels. Camera temperature remained stable and locked throughout the experiment at -70 °C.

All data collected were processed using a MATLAB algorithm designed by another Burrows Lab member. The MATLAB code enables the program to essentially sum the control intensities to help establish what the baseline would be like if both single strands were in the same solution before formation of the heterodimer (*i.e.*, (donor, alone) + (acceptor, alone) = baseline as if they were in same solution). This was done to determine the actual signal enhancement.

Results and Discussion:

Figure 3.3: Percent enhancement in relation to spacer length for 3′Cy3 and 5′Cy5 Pair. The first number is the spacer length on 3′Cy3 reporter and the second number is the spacer length on the 5′Cy5 reporter.

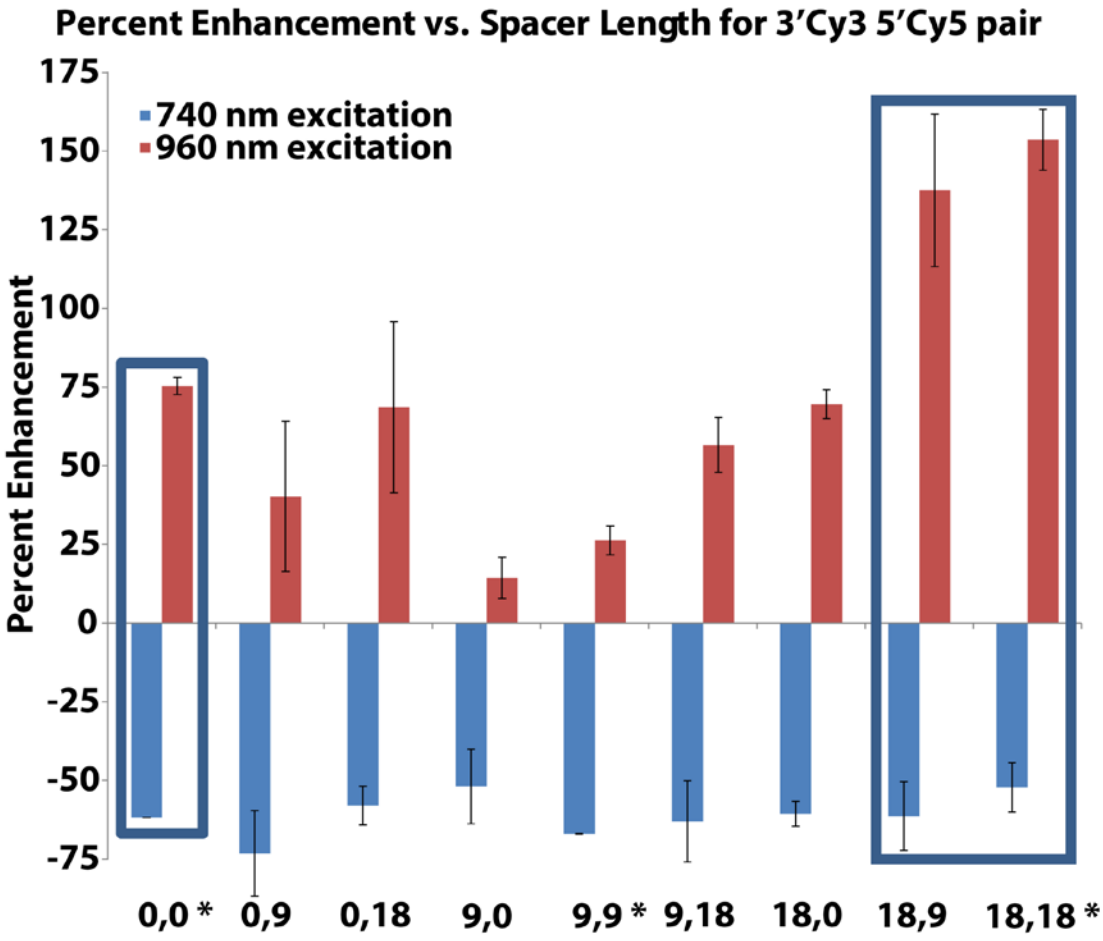

Figure 3.3 illustrates that hybridization of all linear reporter strands excited with 740 nm displayed quenching (blue bars). Quenching is evident by negative percent enhancement of at least – 50 %. On the contrary, excitation at 960 nm, exhibited fluctuating levels of percent enhancement depending on the spacer length and type of combination with another spacer. When linear strands of reporters with 3′Cy3 and 5′Cy5

had spacers of 0 and 0, respectively, it produced an enhancement of about 75 %. When the 3′Cy3 0-spacer reporter was paired with either a 9 or 18 spacer on the 5′Cy5 reporter gave statistically similar enhancements near 50 %. However the signals were very weak as indicated by the large error bars. It was not ideal to have 9 carbon-oxygen spacers on the donor 3′ Cy3 strand and 0 spacers on the 5′Cy5 acceptor strand because this resulted in the lowest percent enhancement: about 20%. Having 9 spacers on both strands also demonstrated an un-ideal outcome, with a percent increase of only 25%. Having a 9 spacer on the donor 3′Cy3 strand paired with an 18 spacer on the 5′Cy5 acceptor strand displayed a very similar percent enhancement as having an 18 spacer on 3′Cy3 donor and a 0 spacer on the 5′Cy5 acceptor. Surprisingly, spacers “18, 9” and “18, 18” produced two of the greatest percent enhancements in comparison to all other couples: ~135 % and ~155 %, respectively.

A closer investigation with spacer combinations of “0, 0”, “18, 9”, and “18, 18” were selected as the top three contributors of increased percent enhancement. To ensure these observed enhancements were not a statistical anomaly the experiments were repeated in triplicated on separate occasions. Figure 3.4 is a bar graph with a side-by-side percent enhancement comparison of the selected top three spacer combinations.

Figure 3.4: Bar chart of percent enhancement evaluation with respect to spacer lengths of "0, 0", "18, 9" and "18, 18".

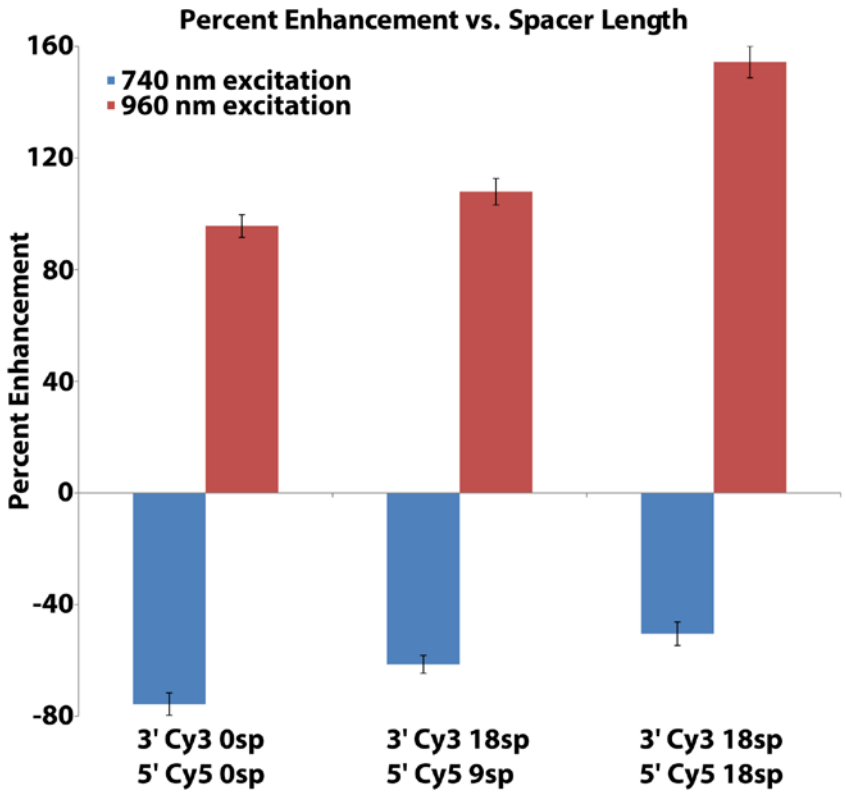

When the selected spacer combinations are placed onto a side-by-side view, there is a clear depiction that the addition of spacers does have an effect on percent enhancement, thus varying lengths of carbon-oxygen spacers do influence the amount of FRET and quenching that occurs with a specific heterodimer. Figure 3.4 shows that with increasing spacer lengths, there was an increase in percent enhancement. In addition, longer spacers correlated with less quenching.

Figure 3.5: Emission spectra at 960 nm excitation of 3′Cy3 and 5′Cy5 pair with “0, 0”, “18, 9” and “18, 18” spacers.

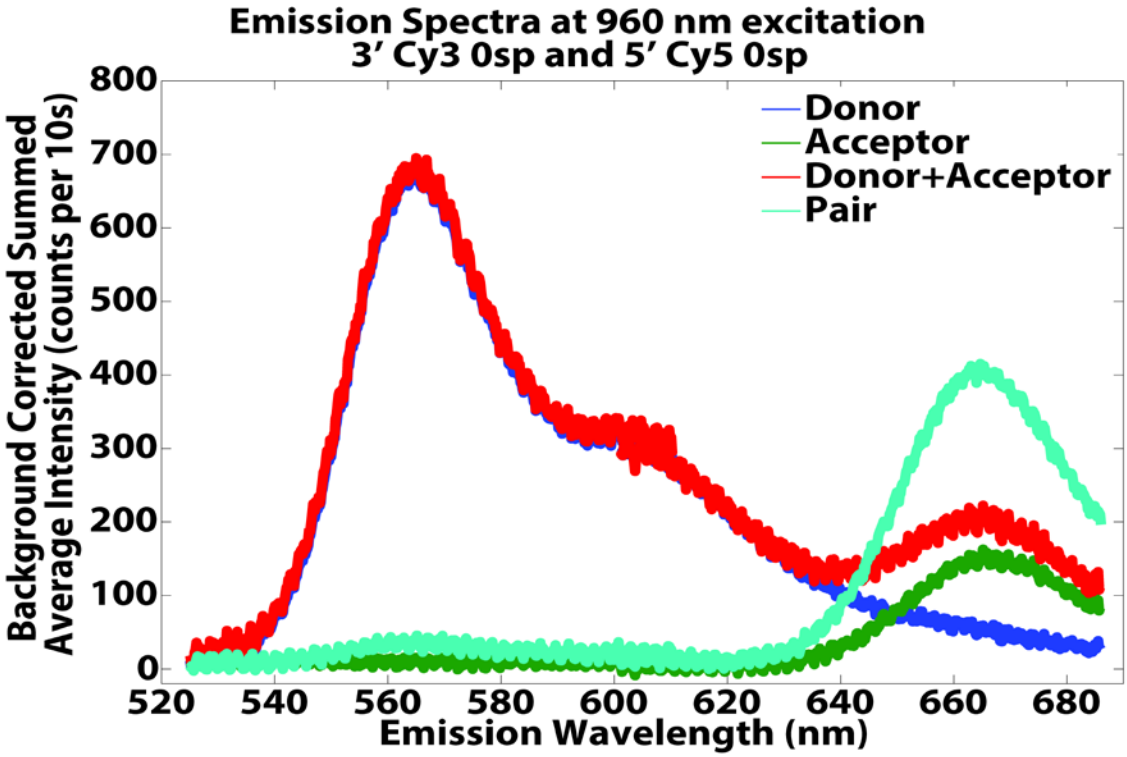

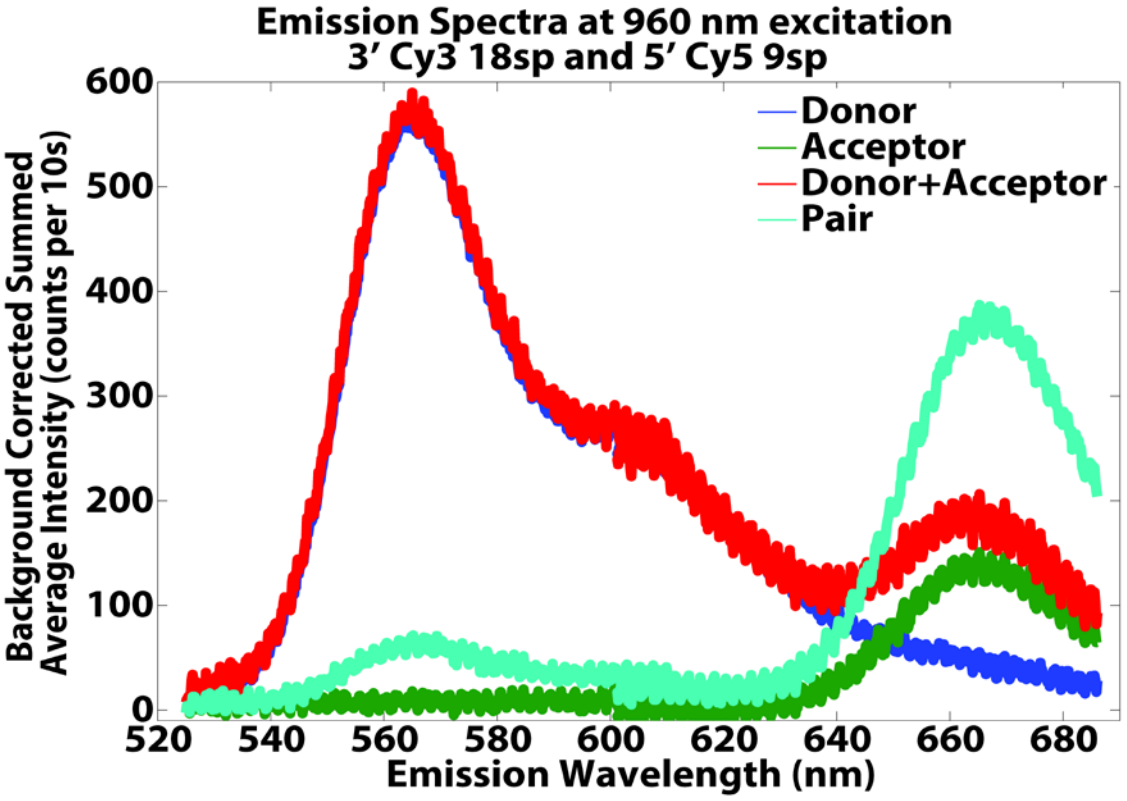

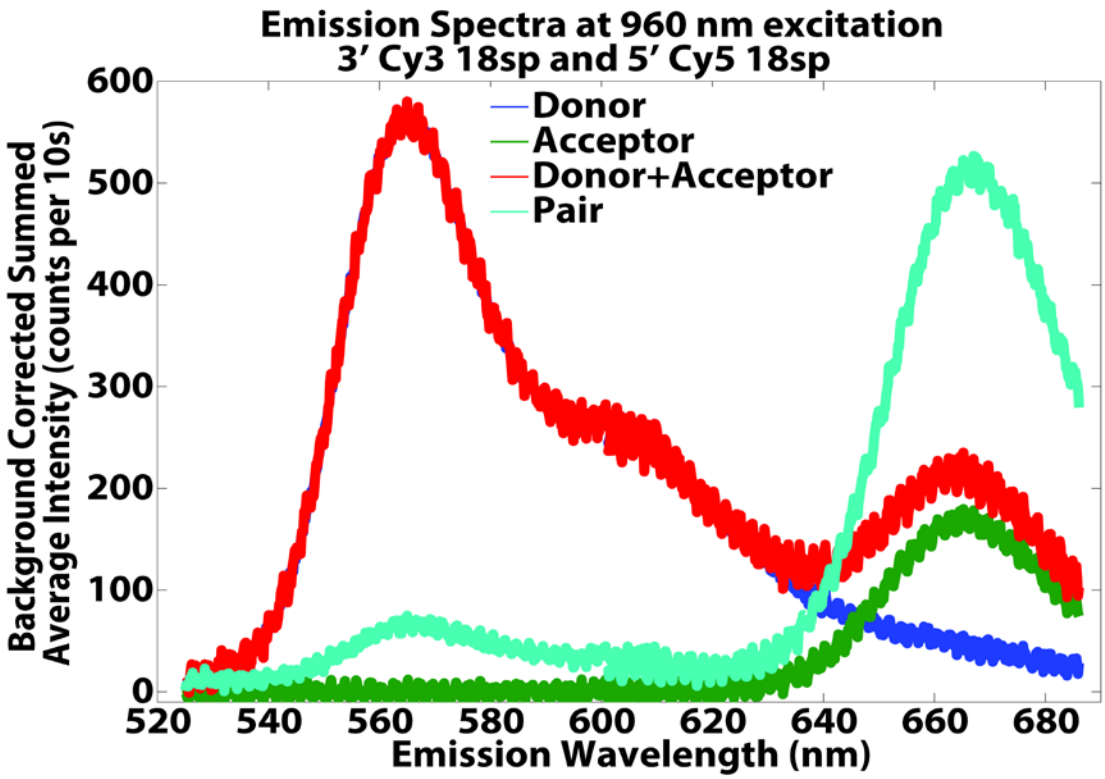

Emission figures, from Figure 3.5, created from the MATLAB algorithm were used to calculate the percent signal change in Figure 3.4. The longer the lengths of the spacers attached to the linear strand reporters, the greater the average Cy5 intensity in counts per 10 s. Analyzing the emission spectra at 960 nm excitation, the blue 3′Cy3 (Donor) and green 5′Cy5 (Acceptor) signals correspond to average intensity counts from each dye individually. The 3′Cy3 emission range extends from 540 – 670 nm, while 5′Cy5 emission region ranges from about 620 nm – 690 nm. The "pair" was the hybridized solution demonstrating characteristic peaks like those of 3′Cy3 and 5′Cy5. Summing the individual Cy3 and Cy5 signals gave the red line. This red line is a simulation of the concept of what the analytical signal intensity would be like if the two single strands were in the same solution. In all three scenarios with the different spacers, the peak in the 3′Cy3 emission region decreased drastically, whereas the peak in the

5′Cy5 emission region demonstrated an increase in average intensity when comparing the differences from the Cy3 and Cy5 emission regions of the “Donor + Acceptor” curve to the “Pair” curve. This drop in Cy3 emission region and rise in Cy5 average analytical signal intensity (Seen in the “Pair” curve) signifies the energy transfer from 3′Cy3 to 5′Cy5. The increase in Cy5 signal was measured as the percent enhancement, such as those seen in Figure 3.4. Figure 3.5 showed that excitation with 740 nm gave quenching of Cy5 signal indicating FRET did not occur. Figure 3.6 confirms the Cy5 signal was indeed quenched but very strong and swamped out the Cy3 signal.

Figure 3.6: Emission Spectra at 740 nm excitation of 3′Cy3 and 5′Cy5 pair with “0, 0”, “18, 9” and “18, 18” spacers. Cy5 signal so strong the Cy3 signal is hard to see.

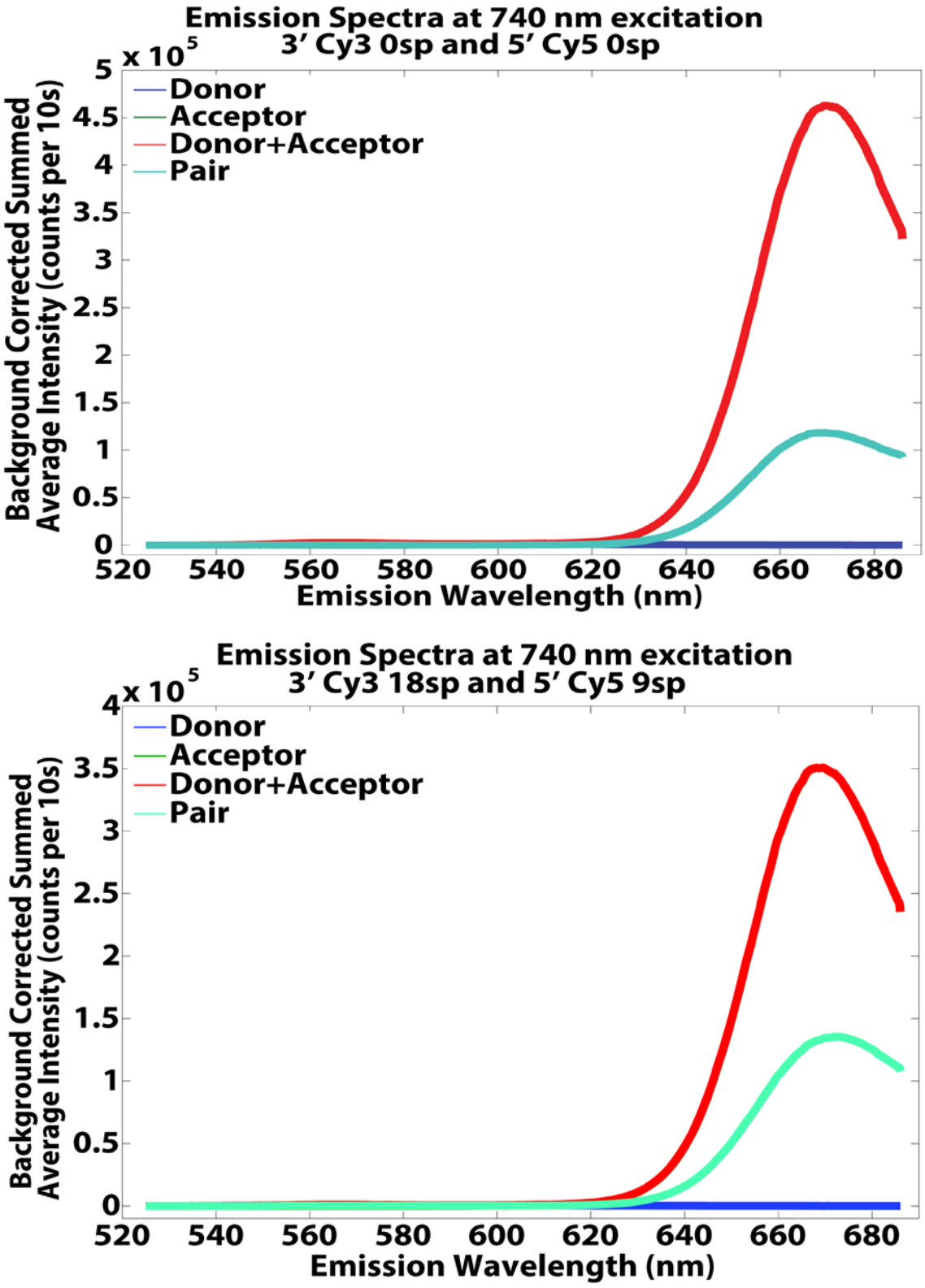

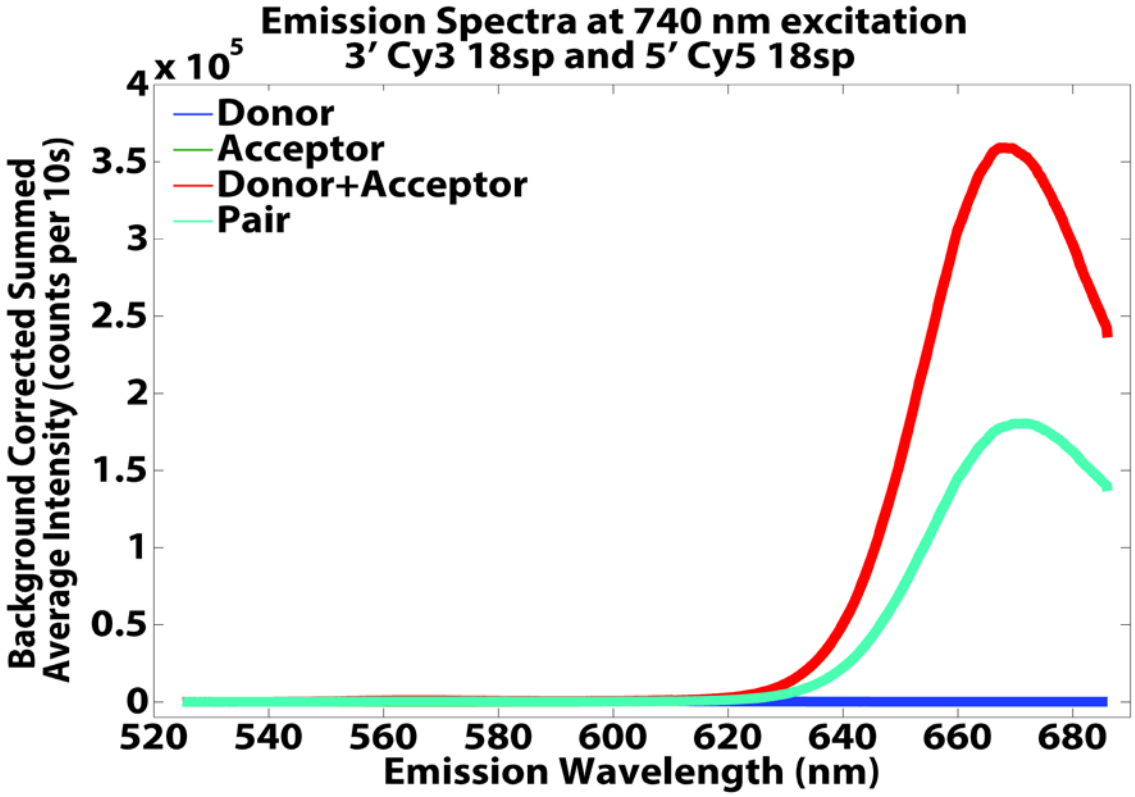

Section 3.0 Conclusion:

From the FRET spacer study, we were able to discover that carbon-oxygen spacers do influence FRET and quenching to a certain degree depending on the length of the spacers. Our results from 960 nm excitation showed that in some cases FRET enhancement improved by increasing the spacer length between the reporting dye and the terminal nucleotide on the single-strands of oligonucleotides. In addition to an increase in average intensity, increasing spacer length also decreases the amount of quenching when excited at 740 nm. Overall, the top three combination of spacers that resulted in the highest analytical signal intensity were: “0, 0”, “18, 9” and “18, 18” spacers—the left

number reflecting the spacers on the donor (3′Cy3), and the right number portraying the spacer number on the acceptor (5′Cy5). Currently in the Burrows Lab, there is ongoing working to utilize these findings in order to design a favorable reporter-probe sensor that is signal-on with Cy3 and Cy5 at different spacer lengths.

Summary

The characterization of the reporter-probe biosensors can be divided into two main incidences: First, we demonstrated proof-of-principle of the reporter-probe biosensor design to selectively detect miRNA. These results confirmed that use of the DNAMelt Web Server to calculate the Gibbs values of reaction aids in predicting that the sensing mechanism will work. The results produced negative values, meaning according to the Gibbs energy, the reaction will proceed to the right forming reporter hairpin structures, in addition to the probe-target complexes. Moreover, our observations displayed that the reporter-probe complex had a decrease in false positive signals after subjecting the reporter-probe biosensor and other commercial models of biosensors in a solution containing endonucleases. In another experiment, I tested the detection limitations of the biosensor (*i.e.*, sensitivity). The results showed that the reporter-probe biosensor was capable of detecting small amounts of miRNA down to the nanomolar level for let-7a, miR-26a, and miR-27a.

It is ideal for a biosensor to have negligible false signals as well as having the ability to detect small amounts of miRNA because, in the body, miRNA is naturally expressed in the femtomolar to nanomolar amounts. Furthermore, early onsets of disease

tend to have low levels of miRNA. Minimal false signals are need because we want to be able to accurately determine changes in miRNA expression without losing the signal in the background.

Furthermore, our studies revealed that the first generation of the reporter-probe biosensor was actually a signal-off type sensor, rather than our predicted and intended signal-on type. Nonetheless, these findings were still beneficial due to the nature of Let-7a. Let-7a is down-regulated in cancers, thus when dealing with Let-7a, it would be more beneficial to have a signal-off sensor to detect the absence, rather than the presence, of Let-7a. That is not to say having a signal-on biosensor is useless, because there is still a demand for signal-on biosensors for detecting the presence or increase of miRNA that are indicative of disease.

The reporter-probe biosensors were also tested for their selectivity. When exposed to a few nucleotide variants or nonsense miRNA in the solution, I found the biosensor still remained highly selective towards the analyte of interest. The fact that the slopes of calibration curves for various miRNA with and without off-analytes were similar provides convincing evidence that the reporter-probe sensors are very selective for their target miRNA. MiRNA exist in families with very similar nucleic acid sequences, therefore, it is important for a biosensor to embody good selectivity because it may need to distinguish between miRNA that are all identical except for one or two bases.

Lastly, several single-strand reporters were paired to test which pair would display the greatest percent change in signal enhancement. It was discovered that the large percent change increase in signal occurred with the 5′Alex488/3′Atto633 pair when excited at 922 nm. From these studies the 5′Cy5/3′Cy3 pair demonstrated the least

enhancement when excited at 952 nm. To encourage better FRET enhancement, a study was conducted using carbon-oxygen spacers placed in-between the ends of the oligonucleotide strands and the dyes. An observable pattern was seen as the spacer lengths increased, so did the amount of FRET enhancement. Not to mention, there was a decrease in quenching as spacer length increased.

Although the reporter-probe biosensors designed in this lab demonstrated high selectivity, sensitivity, and reduced false positives there is still plenty room for improvement. The findings resulting from these studies will be contributed to the ongoing efforts of the Burrows Lab to design an optimal biosensor embodying the beneficial discoveries found through these studies. That said the reporter probe is showing great promise with high sensitivity, selectivity, negligible false positive errors, as well as dual signal-on and signal-off functionality depending on dye pairs used. In fact because of the nature of FRET in the FAM/Atto633 reporter the donor functions as a signal-off sensor while the acceptor functions as a signal-on sensor.

References

(1) American Cancer Society. CancerStatistics 2015. http://www.cancer.org/acs/groups/content/@editorial/documents/document/acspc-044524.pptx (accessed May 21, 2015)

(2) Reyes De Corcuera, I. J.; Cavalieri, P. R. DOI: 10.1081/E-EAFE 120007212

(3) Johnson, N. B; Mutharasan, R. *Analyst*, **2014**, 139, 1576-1588.

(4) Serpico, D.; Molino, L.; Di Cosimo, S. *Cancer Treat. Rev.* **2013**, 40, 595-604.

(5) Larkey, E. N.; Almlie, C. K.; Tran, V.; Egan, M.; Burrows, M. S. *Anal. Chem.* **2014**, *86*, 1853-1863.

(6) Ventura, A.; Jacks, T. *Cell*, **2009**, 136, 586-591.

(7) Gao, J.; Li, L.; Wu, M.; Liu, M.; Xie, X.; Guo, J.; Tang, H.; Xie, X. *PLoS ONE*. **2013**. 8(6), e65138.

(8) Tang, W.; Yu, F.; Yao, H.; Cui, X.; Jiao, Y.; Lin, L.; Chen, J.; Yin, D.; Song, E.; Liu, Q. *Oncogene*. **2014**. 33, 2629-2638

(9) Allcock, P.; Andrews, L. D.; *J. Chem. Phys.***1998**. 108(8), 3089

(10) Integrated DNA Technologies. Fluorescence and Fluorescence Applications Quick Look. https://www.idtdna.com/pages/docs/quick-looks/quick-look---fluorescence-and-fluorescence-applications.pdf?sfvrsn=1 (accessed May 21, 2015).

(11)DINAMelt mfold.rit.alban.edu [http://mfold.rna.albany.edu/?q=DINAMelt] (accessed May 21, 2015)